Article

Finite Element Method in Assessing Strength Properties of a Railway Surface and Its Elements

Jacek Kukulski, Marianna Jacyna *[ID] and Piotr Gołębiowski[ID]

Faculty of Transport, Warsaw University of Technology, 00-662 Warsaw, Poland
* Correspondence: maja@wt.pw.edu.pl

check for updates

Abstract: Development of railway infrastructure at the turn of the 20th and 21st centuries, as well as the speeds of trains in passenger and freight traffic are the result of improving the structure of modern rail vehicles and railway infrastructure optimization. The structure of the railway surface, which enables high speeds and transferring ever greater loads and pressures of up to 25–30 t/vehicle axis, must meet very strict strength and durability requirements. This paper discusses mathematical and numerical tools used in simulation and experimental tests of railway surfaces, as well as its selected elements. Issues addressed in this paper concern, among others, modeling of the railway track, calculations related to its static and dynamic loading, and simulation of the technological process of selected elements of railway turnout. Selected results of the simulation tests on numerical models showing their behavior under different loads are also presented in this paper. The concept of symmetry is included in the possibility of applying the method described in the article both for testing other sections of railway lines, as well as for testing other elements in which stresses occur.

Keywords: railway infrastructure; railway surface; finite element method (FEM); simulation tests; experimental tests

1. Introduction

Development of railway infrastructure observed at the turn of the 20th and 21st centuries, as well as the speeds of trains in passenger traffic up to V_{max} = 300–350 km/h, and freight traffic up to V_{max} = 140–160 km/h on selected lines, are the results of railway vehicle design improvement and railway infrastructure optimization [1,2]. The structure of the railway surface enabling achieving such speeds and transferring ever greater loads and pressures of up to 25–30 t/vehicle axis, must meet very strict strength and durability requirements. The railway surface is subjected to complex dynamic effects during operation, the nature of which changes as load and speed increase.

Over the last several decades, the classic structure of the railway surface has not been subjected to any significant changes. Nevertheless, it should be noted that there has been continuous research and improvements aimed at increasing the safety of railway traffic [3,4], as well as reducing the costs of its maintenance.

Over several decades, a considerable number of research works were conducted and a considerable number of books and papers were published, both domestic and foreign, whose subject matter included modeling of the surface and its components.

Railway transportation, being one of the safest modes of transport, requires ongoing research on structural solutions optimization. Research is necessary due to the high requirements posed in the certification process and pre-commissioning approvals, and due to the considerable costs of constructing infrastructure. Increases in safety and reduction in operating costs are achieved through diagnostic works carried out on elements of railway infrastructure.

In contemporary railway transportation, developing computer models and simulations employing third party or proprietary computer software is a common practice. This is due to the complexity of processes and phenomena in elements of railway infrastructure, specifically at the contact between the wheel and the rail.

One of the objectives of this work is to present original models of railway infrastructure elements with the finite element method (FEM), and to conduct simulation studies showing the impact of technological processes in the production of railway turnouts on the distribution and the amount of residual stresses in steel components of railway infrastructure [5,6]. The second research area is simulation research of the experimental railway surface aimed at limiting deconsolidation process and extending its service life as well as reducing operating costs. The concept of symmetry is included in the possibility of applying the method described in the article both for testing other sections of railway lines, as well as for testing other elements in which stresses occur.

In addition to simulation tests, this paper also includes selected experimental studies carried out by one of the co-authors.

2. Literature Review

The finite element method is widely used in solving various engineering problems. Its universality consists in the relative ease of creating a description of different areas and shapes with complex geometry.

The finite element method allows the strength of the structure to be studied and the simulation of deformations, stresses, displacements, and heat and liquid flows [7]. It is widely applied in various fields where the adaptation of the material type to the load being transferred plays an important role. Such systems are also found in rail transport—more specifically in the issues related to railway line infrastructure, as well as in the place where the elements of railway superstructure and infrastructure meet.

The railway surface is a very important element for the train's movement. It transfers the stresses caused by the passing vehicle [8]. Therefore, it has a very important function—to absorb vibrations in a way not affecting passing rolling stock, and thus the passenger's comfort of travel. For several decades, numerical methods have been used in research on railway track elements. Intensive work was conducted at the Warsaw University of Technology, Cracow University of Technology, and other research centers in the country and abroad [3,9–11]. Those works covered analysis of residual stresses in elements of steel turnouts, i.e., rails and needle profiles. The main purpose of numerical calculations was to determine residual stresses remaining in the rail after unloading and to determine impact of various parameters on the magnitude of those stresses and their distribution in the material. Obtained results of numerical calculations were compared with the results of stress measurements made with the ultrasonic technique.

Desai and Siriwardane [12] present numerical models for track support and structures. Authors presented in detail three finite element formulations based on one, two, and three-dimensional idealization for analysis of railroad track support structures, with major emphasis on the three-dimensional procedure.

A lot of information on the use of the finite element method to analyze stress generated in the railway surface can be found in the literature. The research can be done both in two-dimensional space and three-dimensional space [13,14]. The works [3,15–17] are related to the modeling of phenomena arising as a result of rolling rails on rollers and other levelers. In works [3,18,19] rail models and distribution of residual stresses after rolling simulation were presented. Influence of the rolling process on the size and distribution of stresses was also determined. The finite element method, as a basic computational tool in modern mechanics, was also applied to the issue of track, track bed, stabilized ballast and vibroinsulating mat [20,21] or track and ballast [22–24], and joint action of different types of surface. An important group of studies is related to the research on dedicated surfaces, as seen in [14,25–29] and others.

Some studies concern specific infrastructure facilities in which various types of surfaces are in contact, such as bridges and tunnels. In the paper [30], research was conducted on a railway bridge on the siding to the "Bogdanka" Coal Mine. The ABAQUS software was used for the FEM analysis. Detailed calculations also allow the selection of the right type of surface for the transition zone in front of or behind the bridge [31]. The second type of specific infrastructure elements are tunnels, in which the railway surface also affects the structure of tunnel facility. Problems related to the exploitation of the surface in tunnels were described in [32].

Research with the FEM can also help to assess the condition of facilities, including the railway surface, after problematic situations. In the paper [33], research on a railway viaduct damaged by mining damage was described. The FEM also allows the best solution in a given place to be chosen [34]. It should be noted that this was also done by optimization methods [35].

An important group of studies on the use of the finite element method for analysis of railway surfaces focus on issues of the vehicle's interaction with the surface. In the paper [36], an analysis of the wheels' interaction with a flexible track mounted on bridges was conducted.

Classic railway surfaces constitute a railway grid consisting of rails and sleepers immersed in the ballast layer lying on the track bed. They work under operating load in the elastic–plastic state. The source of permanent–plastic deformations is ballast. Modern technological and material achievements make it possible to work the track bed under operating load in an elastic state [11,20,37]. The weakest element of classic railway structure is the mechanically compacted aggregate layer. Dozens of research works on the quality, type, and composition of the aggregate have been conducted [36]. Many works were also conducted on the method of mechanical compaction of the aggregate ballast [38]. However, there are still unsatisfactory results in reducing the intensity of irregular uneven permanent deformations of the ballast. As a consequence, there is a need for systematic and frequent repairs of unacceptable geometrical inequalities of the track. The contact of the wheel with the rail generates energy, which is transmitted through the rail and fastening of the rail to the sleeper and then through the ballast layer to the track bed. This creates an intense vibration field. The kinetic energy increases with increasing train speed. As a consequence, the acceleration of the vibrations of rails, sleepers, ballast, and track bed increases. This causes the formation of significant tensile stresses in the ballast, which may affect the balance of internal friction forces causing its fragmentation. Therefore, it is inevitable that ballast subsidence (plastic deformation) occurs. It grows with the increase of stress under the sleeper [39] and along with the increase of vibration accelerations.

The aggregate layer undergoes tensile stress. In addition, vibrations cause acceleration in the ballast layer exceeding g-standard gravity value, which additionally reduces the ballast's resistance to the transfer of tensile stresses.

The gravel layers at the level of contact between the sleeper and ballast under the utilization load are in spatial state of compressive stresses. The main stress tensor is the following relationship: $\sigma 1 > \sigma 2 > \sigma 3 > 0$. This means that the aggregate is in a triaxial state of compression, and therefore the best conditions for the work of ballast are there. The most unfavorable conditions occur where the ballast is exposed to tensile stresses, and they have the character of pulsating variable stresses.

The field of intense vibration, which is formed at the contact between the wheel and the rail, is transferred by individual elements of the surface to the ballast and track bed. It causes tensile stresses, disturbing the existing balance based on the principles of internal friction [40]. As a consequence, it causes fragmentation of the aggregate ballast and its subsidence.

Stresses in the aggregate ballast can be determined in an analytical, as well as a simulation way using different methods and formulas. A closer analysis shows that tensile stresses arise in areas close to the rail fixation—the place of transferring wheel-sleeper-ballast loads—and in areas by the sleeper's front side. The top layer of ballast in those areas requires resistance to deconsolidation hazards. The stress analysis in the rail substrate shows that tensile stresses only disappear in the rail substrate at depth 60–80 cm.

The reduction of stresses in the ballast can be achieved by its complete elimination. It can be done by using a non-ballast surface or looking for innovative technological solutions that strengthen the existing structure with geotextiles, geogrids, and other materials.

Tribology aspects of the railway ballast are a difficult issue and have been addressed only by a few authors. In [41–43], experimental and simulation tests of the ballast, as well as the analysis of phenomena occurring in the ballast under load, were presented.

For many years ORE D182 group research developed certain standards regarding the assessment of aggregates used for railway ballast. In the case of ballast applied on high speed lines of up to 350 km/h, it undergoes tests in the Deval Drum and the Los Angeles ball drum. Those tests allow the assessment of the average abrasiveness and the assessment of breakability in the case of large axle loads.

In addition to experimental research, numerous papers were created in which the authors dealt with the railway ballast and the entire surface simulation tests. The following two trends can be seen. One in which the FEM ballast model in solid form is adopted [3,15,44–46], and one that attempts to build discrete models [47–49].

3. Research Objects

3.1. General Assumptions

The objects of the simulation tests include: steel elements of railway turnouts such as needle profiles, wing rails, and classic and reinforced railway surface models. In the later part of the paper the assumptions for simulation tests, as well as selected results of those tests are presented. Simulation tests were often validated with experimental tests; however, this paper will be limited to only simulation tests. The ABAQUS software [50], on the Warsaw University of Technology license, was used for modeling and simulation tests. ABAQUS has broad possibilities for nonlinear analysis of physical issues, including mechanics of deformable solids.

3.2. Simulation Tests of Steel Elements of the Railway Surface

3.2.1. Test Characteristics

The simulation tests of steel elements of the railway surface include modeling of bending and hardening processes of rail and needle profiles—the component elements of railway turnouts. The bending process aims to properly shape the turnout elements to the arc curvature. On the other hand, the surface hardening is aimed at increasing the hardness and durability of the running surface of the needle profile, which is subjected to significant dynamic loads in operation.

The geometry of the numerical model was defined in the form of a grid of nodes defining the location and size of finite elements. Three-dimensional solid elements were selected. Due to the complex shape of the modeled objects, three-dimensional, solid, cuboidal elements with a triangular base (containing five walls) were introduced in addition to the cuboidal elements containing six walls. The selected elements are shown in Figure 1.
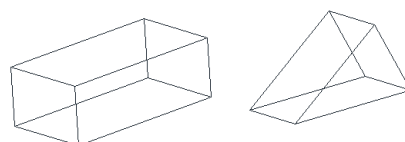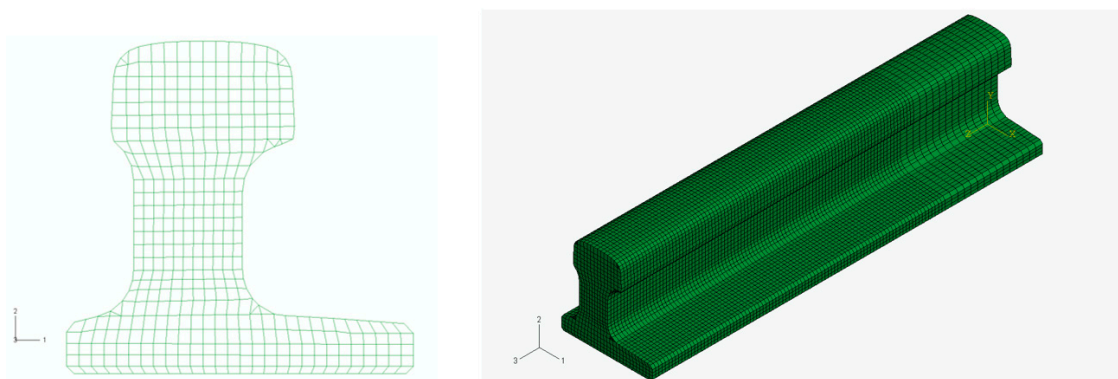

Figure 1. Solid C3D8R and C3D6 elements.

Square elements are considered to be more suitable to describe issues in which bending prevails. They better describe stress concentration and allow better approximation of curved shapes with fewer elements. Figure 2 presents a cross-section of a needle profile model with six- and eight-node elements.

Figure 2. Cross-section and view of the I60 profile model with the C3D8R and C3D6R components elements.

3.2.2. Boundary Conditions and Load

The method of support and load was replaced in the numerical model by idealized boundary conditions. The calculation process was divided into two steps, the first one corresponding to the loading and the second one corresponding to the unloading. In the case of the surface hardening simulation, the first step corresponds to heating and the second one to cooling.

The support conditions are determined in the model by ensuring the appropriate degrees of freedom in the nodes best suited to experience them are present in the support.

Nodes in support cross-sections were selected as the most suitable for the support simulation. The forced displacements are applied to all nodes in the cross-sections where the loading was applied in the experiment (U1 = 15 mm). These cross-sections are marked as Z744, Z604, in Figure 3. For the simulation use model 3D rail I60, the length of object was 1275 mm.
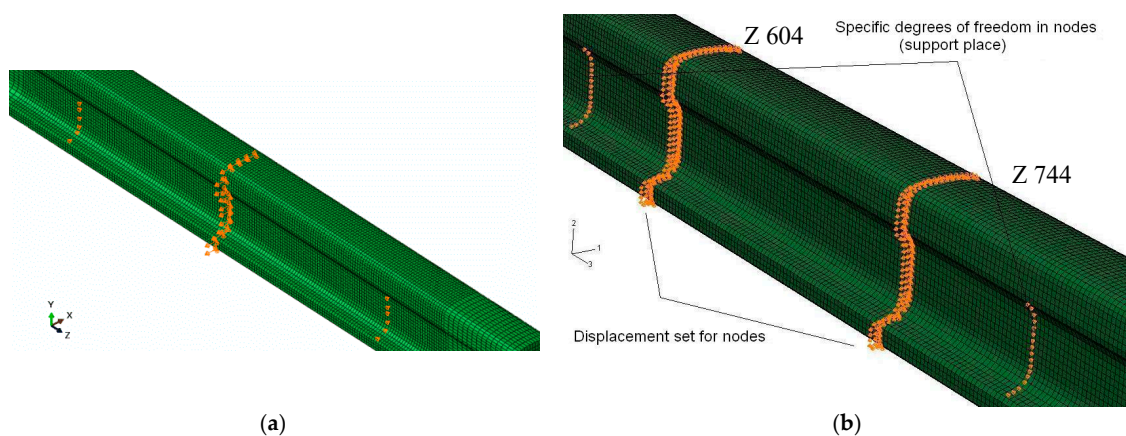
Figure 3. Boundary conditions and load for the I60 three-point (**a**) and four-point (**b**) material model.

Table 1 shows relationship of stress σ and deformation ε for the uniaxial tensile test of rail steel. In addition, for the surface hardening simulation, the effect of temperatures on deformation and stress values was taken into account (Figure 4). The material parameters used in the finite element model (rail 60E1 and I60) were taken from the experimental tensile test.

**Table 1.** σ–ε relationships for axial expansion of rail steel.

Stresses	Plastic Deformation
σ (MPa)	ε (%)
0.0	0.0
629.7	0.4
900.0	2.6
1066.0	6.0
1069.0	16.0
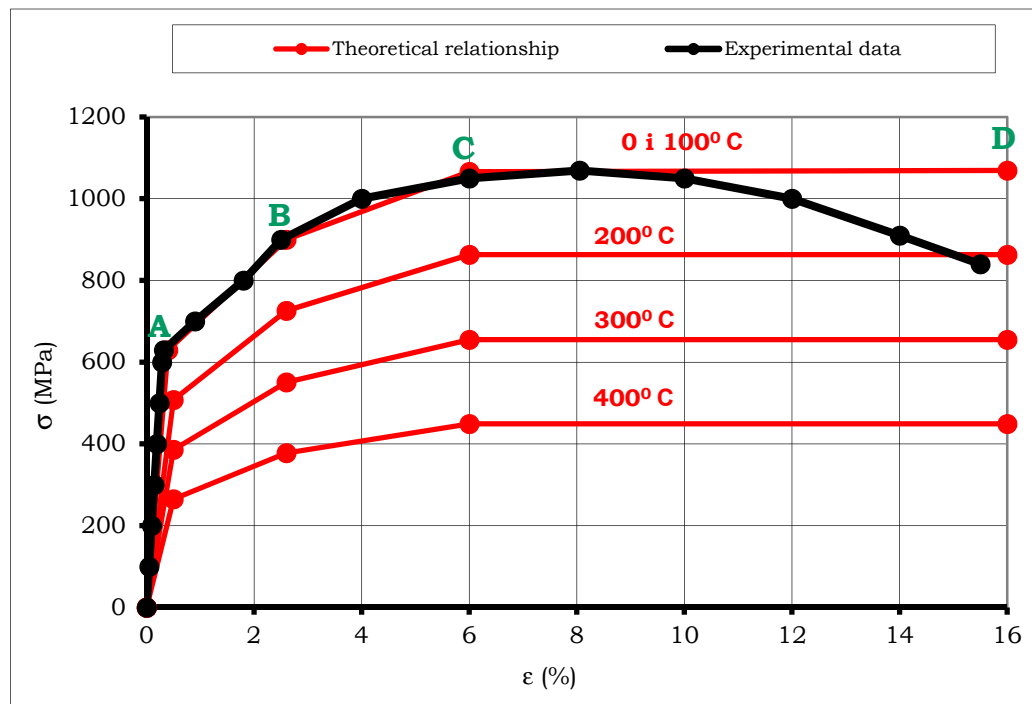
Figure 4. Experimental and theoretical relationship curve σ–ε for axial stretching of steel depending on the heating temperature [45].

3.2.3. Simulation Tests Results

Figures 5–7 present the results of numerical calculations of three-point bending, four-point bending and surface hardening. The drawings show the reduced stress σ^{HM} and the residual stresses σ_{11}.

Obtained results show that differences in stresses in the same cross-sections and measuring points after a four-point bending, while maintaining the same load conditions, are in some cases even 50–100 MPa lower than the three-point bending. The distribution and magnitude of residual stresses is more favorable and more even. In the case of four-point bending in the middle part of the samples, a pure bending between the points of application of the load characterized by the same distribution of stresses along the axis of the sample appeared. The bending process increases residual and tensile stresses. The greatest stresses occur in the head and foot of the profile, because after bending forces have been relieved, the most elastic energy remains in head. In turn, the results of measurements after surface hardening, shown in Figure 7, show that hardening enters into the system an element of compressive stress reaching 160 MPa. This is a beneficial phenomenon because compressive stresses can prevent microcracks in the material structure and other adverse effects.
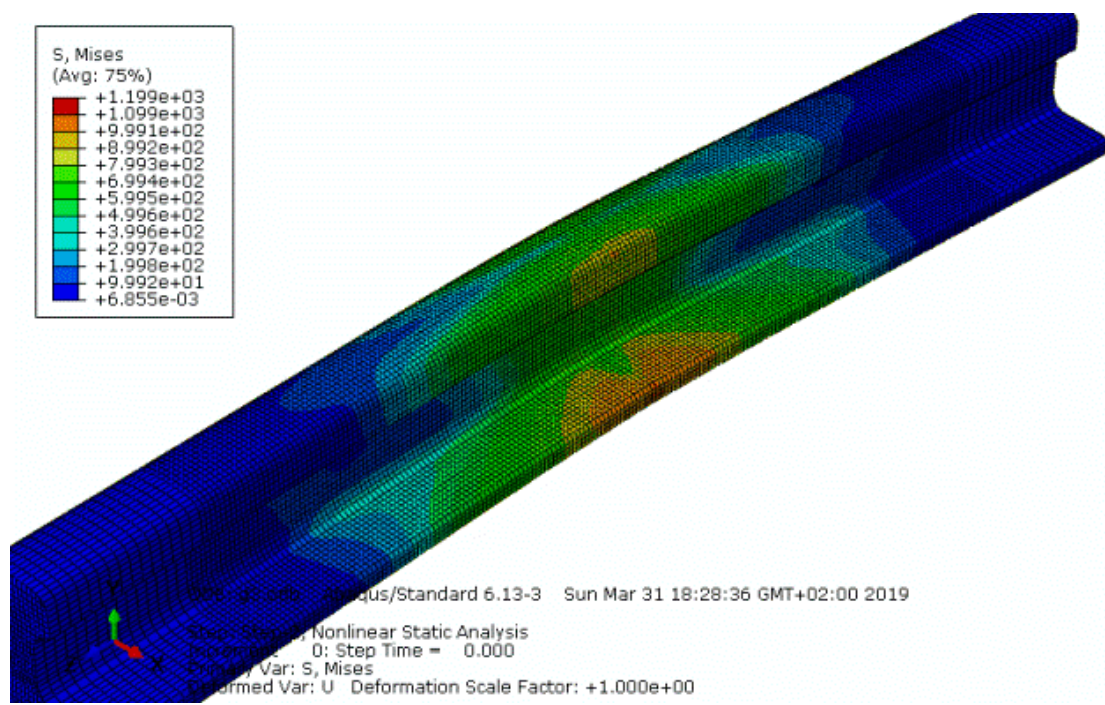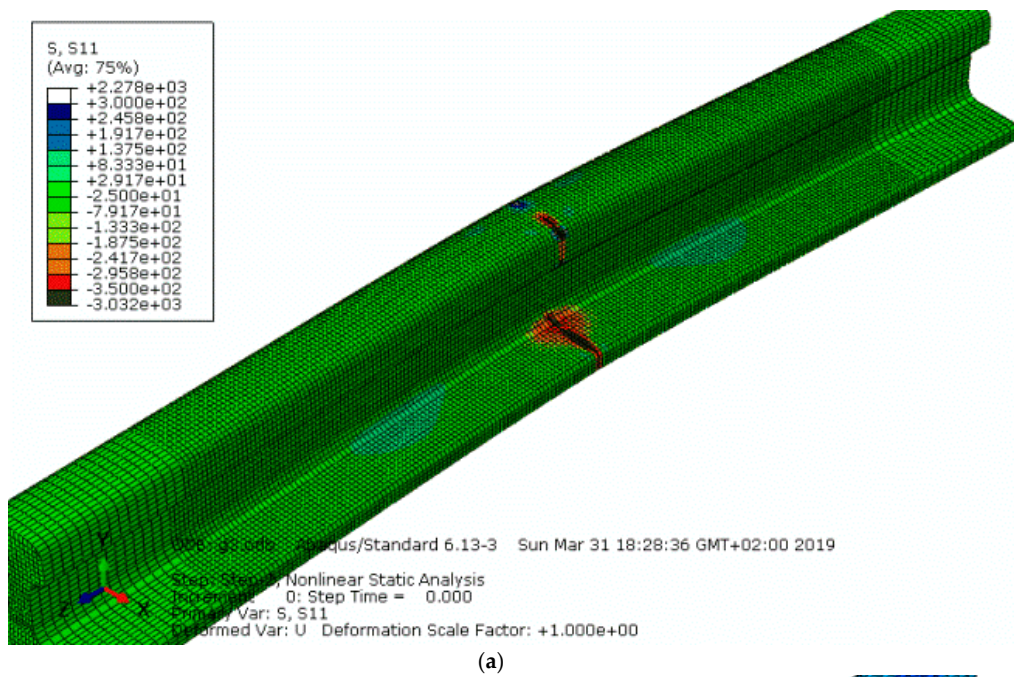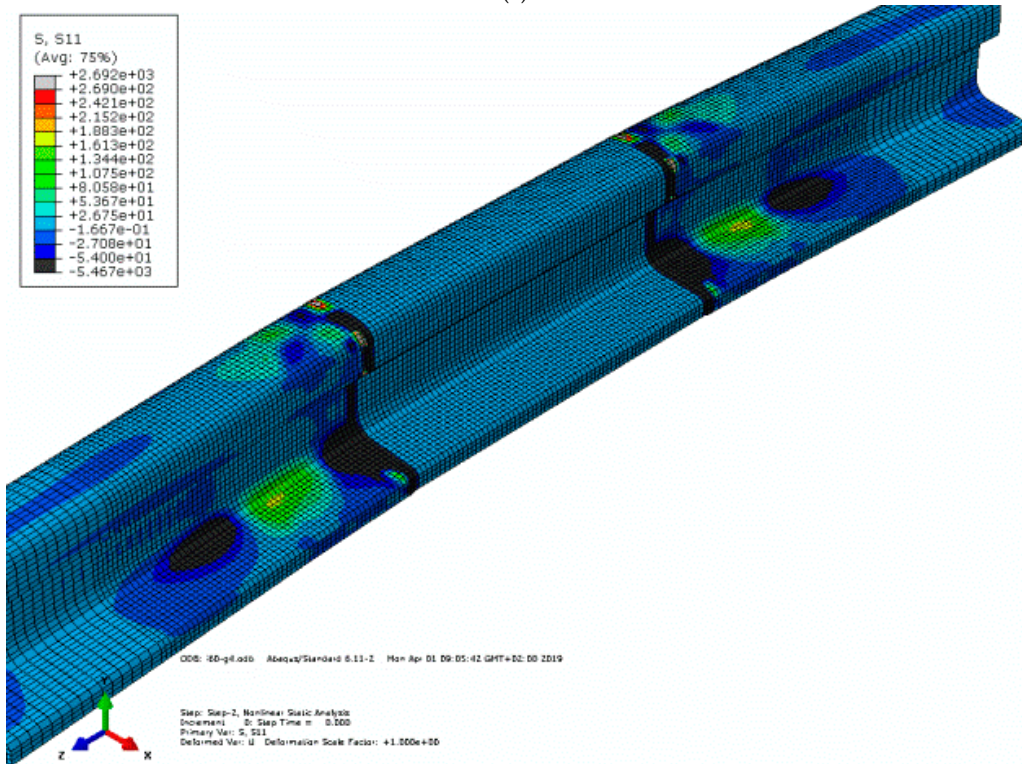
(**a**)
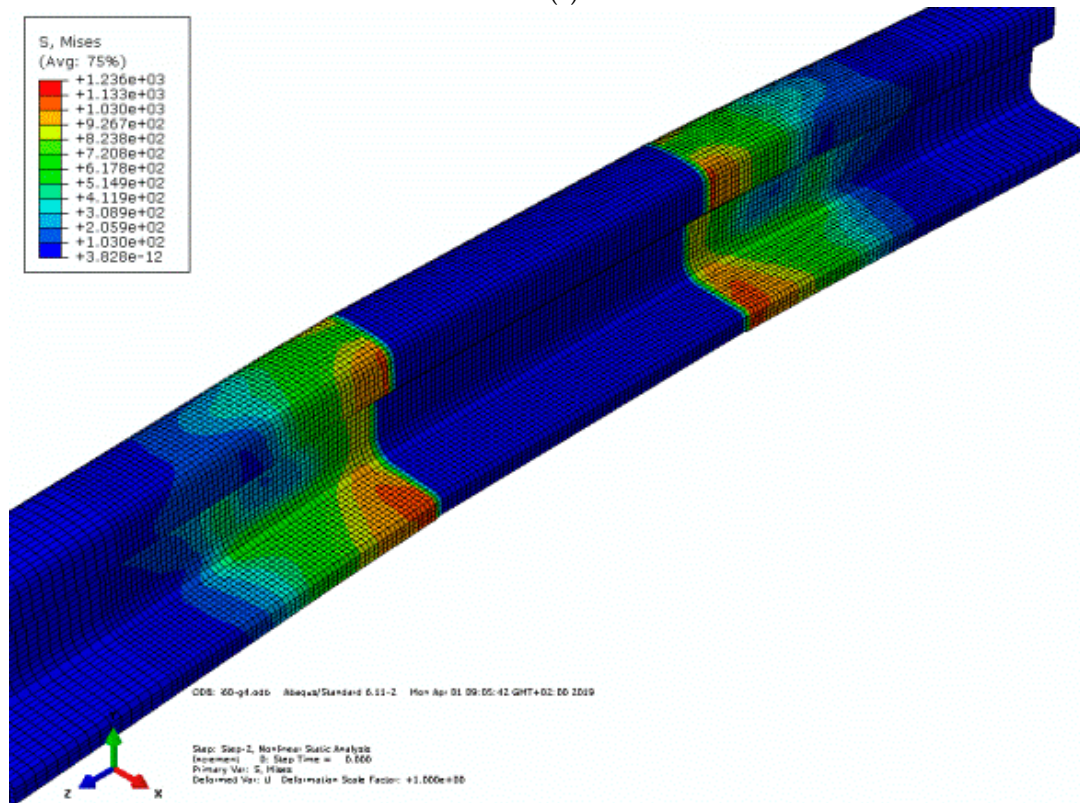
(**b**)

Figure 5. Contours of reduced stress σ^{HM} of the rail I60 after three-point (**a**) and four-point (**b**) bending.

(**a**)

(**b**)

Figure 6. Contours of residual stresses σ_{11} after three-point (**a**) and four-point (**b**) bending of I60 profile.
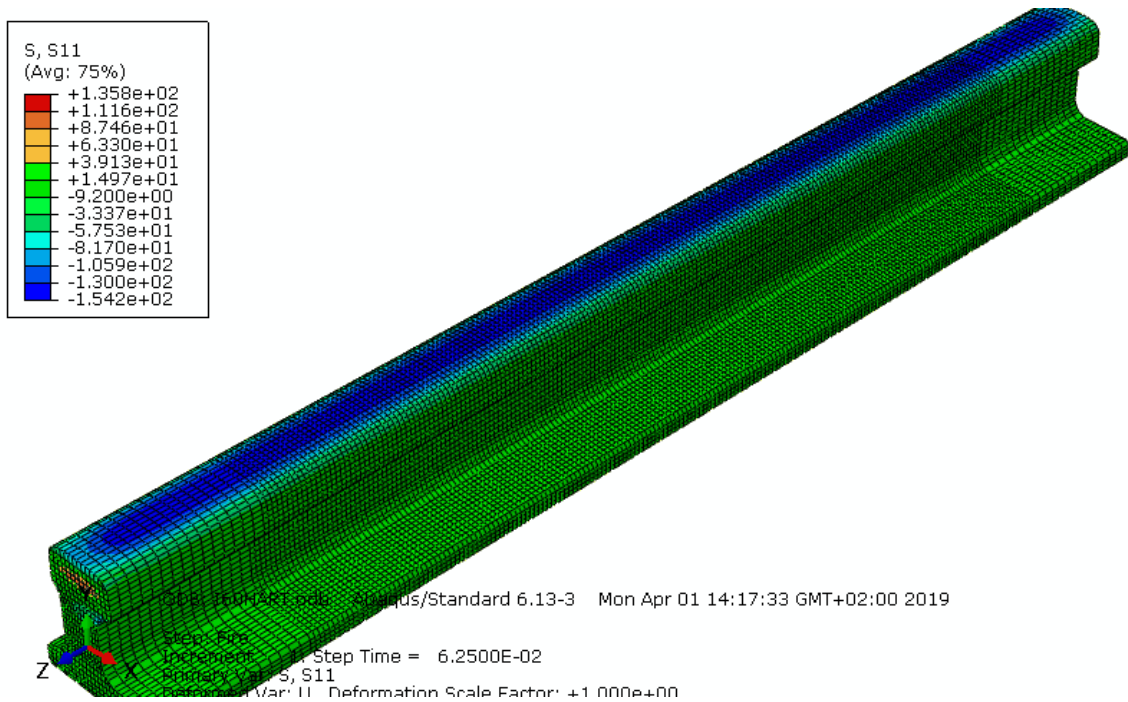
Figure 7. Residual stress contours after surface hardening of I60 needle profile.

3.3. Simulation Tests of the Railway Surface

An extension of the works presented above was the structure of numerical models of the railway surface. Constructed (FEM) models included various configurations of the railway track structure taking into account different load variants. One of the solutions was an innovative solution for the aggregate composite surface developed in the Faculty of Transport of the Warsaw University of Technology [25]. This solution was characterized by a complex reinforcement of the classic ballast surface with the use of geogrids and gluing the top layer of the aggregate with a special polyurethane resin. Figures 8 and 9 show illustrative cross-sections of the railway surface together with the attenuation and elasticity parameters determined between the individual components of track used in simulation tests.
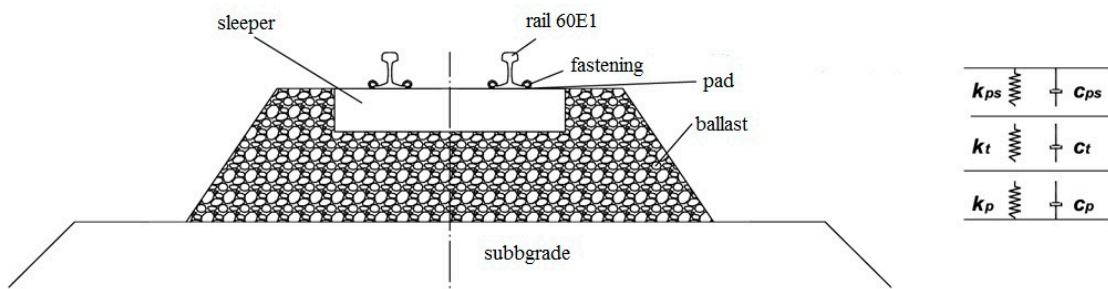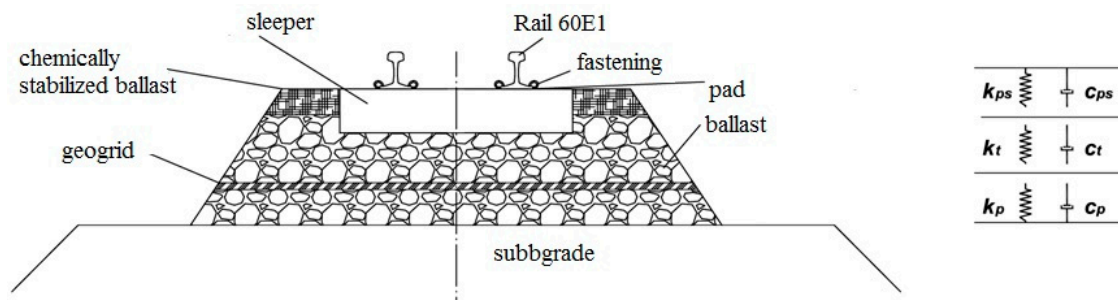

Figure 8. Cross-section of a classic railway surface.

Figure 9. Cross-section of a classic railway surface with additional components.

The equation of motion for the classic railway track, taking into account the load and weight of individual elements, as well as attenuation and elasticity coefficients, can be presented in form of differential equations described in Equations (1) and (2).

$$EI\frac{\partial^4 z_r}{\partial x^4} + m_s\frac{\partial^2 z_r}{\partial t^2} + c_{ps}\frac{\partial z_r}{\partial t} + k_{ps}z_r - k_{ps}z_s - c_{ps}\frac{\partial z_s}{\partial t} = P(t)\delta(x), \tag{1}$$

$$m_s\ddot{z}_s + c_s\frac{\partial z_s}{\partial t} + k_s z_s = k_{ps}(z_r - z_s) + c_{ps}\left(\frac{\partial z_s}{\partial t} - \dot{z}_s\right), \tag{2}$$

where:

EI—bending stiffness,
m_s—rail unit weight,
c—damping,
k—stiffness,
z—displacement,
$P(t)\delta(x)$—extortion.

Track deflections are calculated by solving the equation in an analytical way for previously accepted parameters.

3.4. Boundary Conditions and Load

The support method that occurred during the experiment was replaced in the numerical model by idealized boundary conditions. The pressure of a static or dynamic roller on the rail, as well as the rotational speed of the roller that simulates the vehicle speed is preset. The load is applied gradually (incrementally) and at each step the system of equations is solved in order to determine the increase in stresses, deformations, and displacements. The support conditions are determined by taking away appropriate degrees of freedom, preventing the model from moving in certain directions. In each load cycle, the force F = 112.5 kN (Figure 10) was applied.

In the case of solid models, the grid in individual elements of the surface has a different size. In order to properly perform the simulation calculations, the places of contact between individual elements of the railway surface are defined. Contact between the wheel and rail in the model was defined as the interaction between created surfaces on the wheel and on the head of the rail. Selection of master and slave surfaces defines contact between the entire master surface and the entire slave surface. Surface-to-surface contact with small sliding is considered for all contact interactions in the model which assumed a relatively small sliding. For the simulation calculations, kinematic contact taking into account the coefficient of friction between neighboring planes was used. This allows for proper distribution of pressure on both grids to maintain the homogeneity of the 3D model. Figure 11 shows the contact interfaces used to properly distribute the pressure to individual elements of the model.

(**a**)

(**b**)
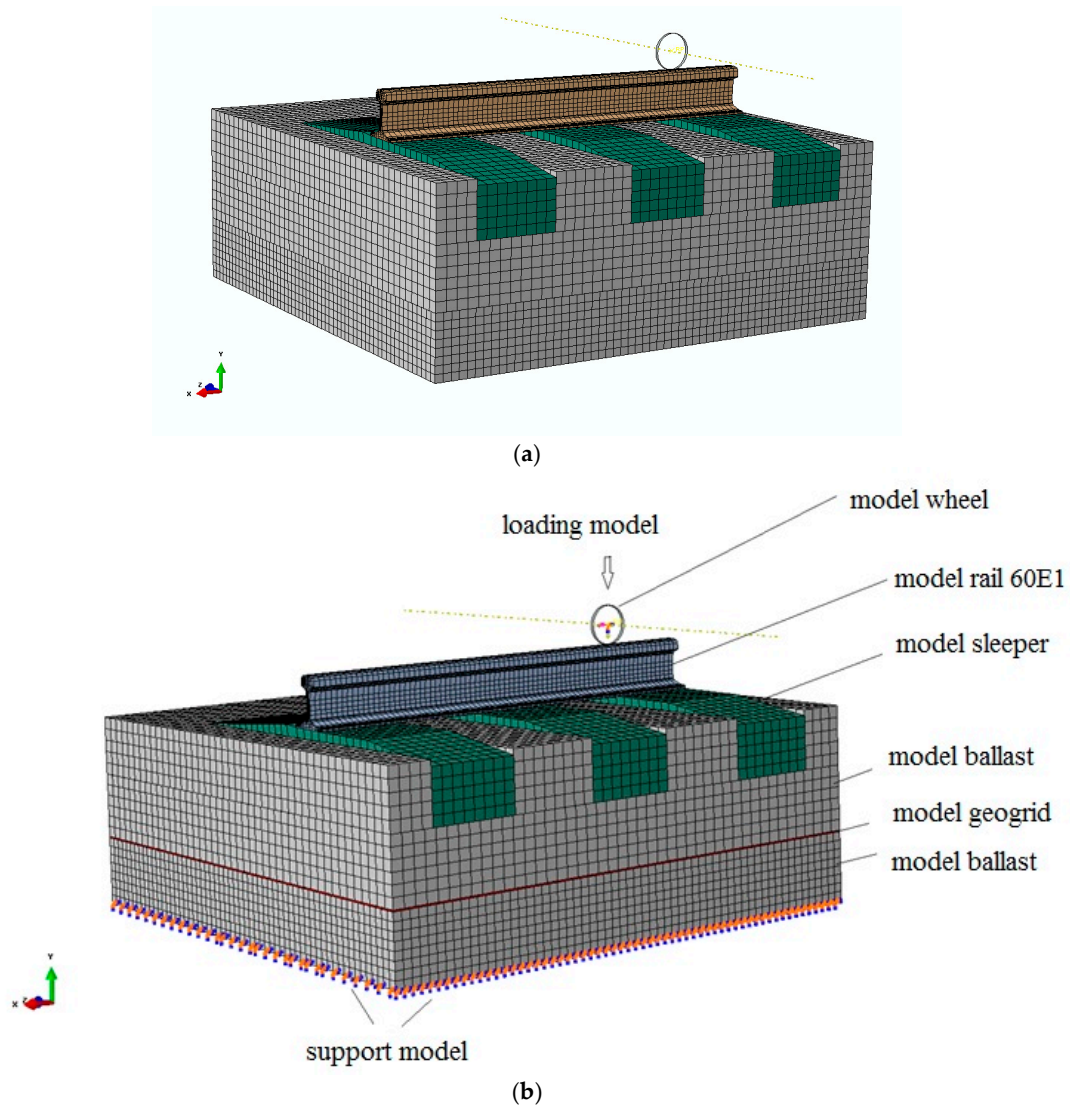
Figure 10. Boundary conditions and load for surface models, (**a**) without reinforcement; (**b**) with geogrid reinforcement.

(**a**)

(**b**)
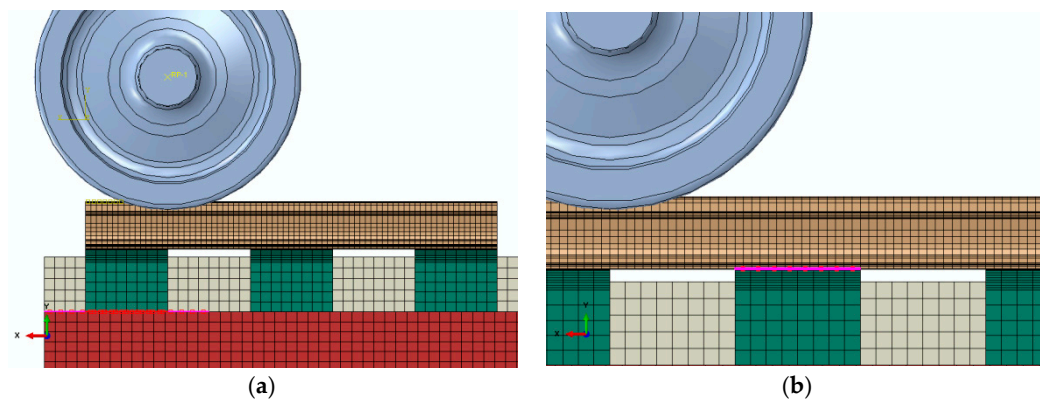
Figure 11. Interfaces between sleeper and ballast (**a**) and rail foot and sleeper (**b**) (one-sided connections).

3.5. Material Models

In the case of numerical models of the railway surface, the stress relationship of σ and deformation ε curves for the rail presented in Section 3.2.3 were used. Tests also took into account the rigidity and attenuation parameters of elements included in the track structure (Table 2). Those values were adopted on the basis of an experimental test of individual elements presented in various scientific publications. For the rail 60E1, the material parameters used in the finite element model were taken from the experimental tensile test. Changes in values of individual stiffness and damping parameters can significantly affect the obtained simulation results.

Table 2. Rigidity and attenuation parameters of the railway track in the simulation tests.

| Designation	Parameter	Value	Unit
E_r	Elastic modulus of 60E1 rail	210,000	MPa
k_{ps}	Rail pad stiffness	78	kN/m
c_{ps}	Rail pads damping	50	kNs/m
ρ_b	Ballast density	54	kg/m^3
ρ_r	60E1 rail density	7850	kg/m^3
E_b	Elastic modulus of the ballast	150	MPa
v_r	60E1 rail Poisson's ratio	0.3	-
v_b	Ballast Poisson's ratio	0.35	-
v_s	Sleeper Poisson's ratio	0.3	-
c_p	Ballast damping	250	kNs/m
k_p	Ballast stiffness	110	MN/m
ρ_s	Sleeper density	2400	kg/m^3
E_s	Elastic modulus of sleeper	70,000	MPa
E_g	Elastic modulus of geogrid	0.57	GPa
v_g	Poisson ratio of geogrid	0.5	-
ρ_g	Geogrid density	0.00132	kg/m^3

3.6. Results of Simulation Calculations

The selected results of numerical calculations, obtained with 3D models of the railway surface in various configurations are presented in diagrams depicting contours of the Huber–Misess replacement deformation, as well as the deformations (deflections) of the model elements. The sample results of numerical calculations are shown in Figures 12 and 13. The calculations were made for half of the surface model and ten computational cycles simulating loads of wheels with a pressure of 112.5 kN.

Based on the simulation tests, it can be noticed that geogrid immersed in the aggregate ballast, at a depth of approx. 20 cm below the foundation, causes a more even distribution of stresses and deformations. Those values are 5–10 percent lower than the classic solution. Extreme stress values occur within and under the sleepers. Another function of the geogrids, in addition to strengthening the entire structure of the track and track bed is to ensure the stability of ballast by anchoring it in geogrid meshes. This ensures even distribution of pressure transmitted from the wheels of rail vehicles through the rail elements and sleepers to the aggregate ballast. Limitations related to the completed test cycles result from a large number of finite elements, significantly extending the simulation time.
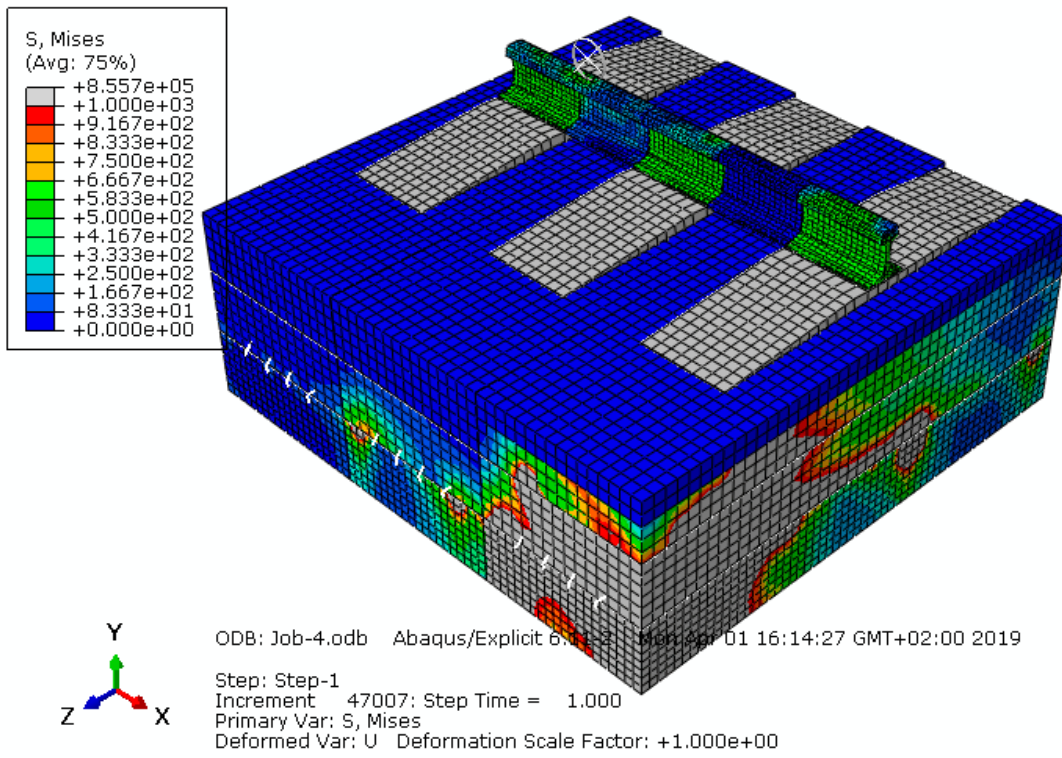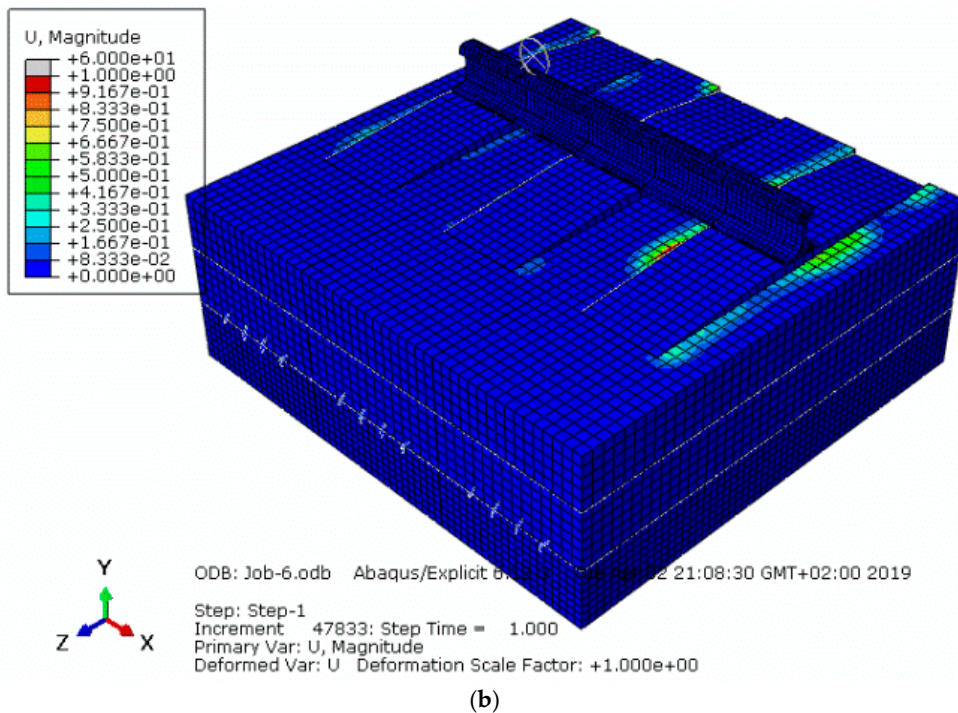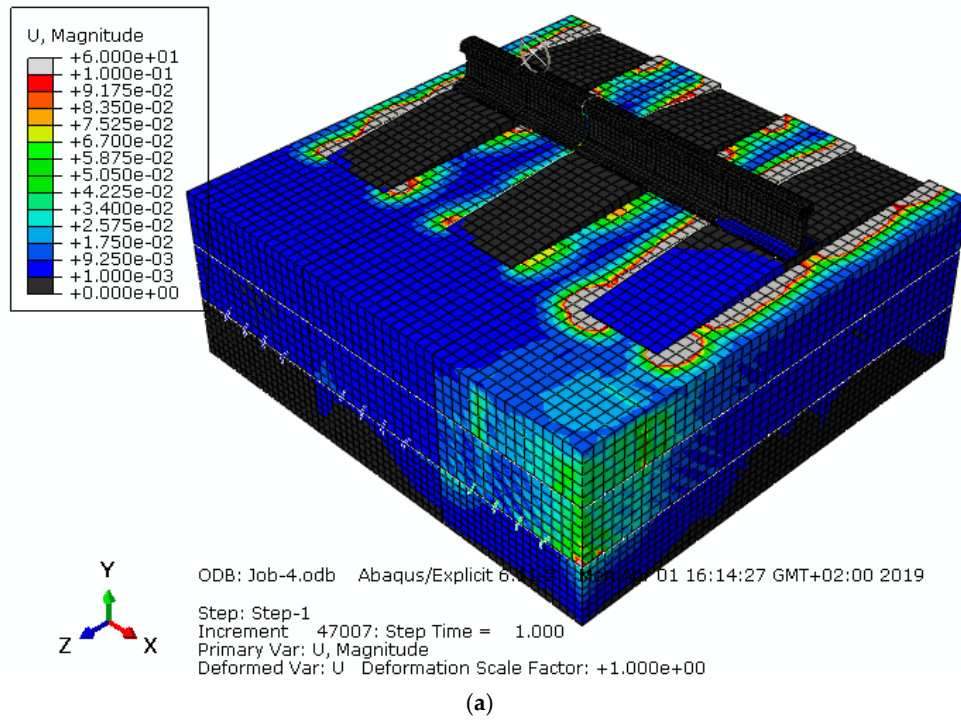
(**a**)
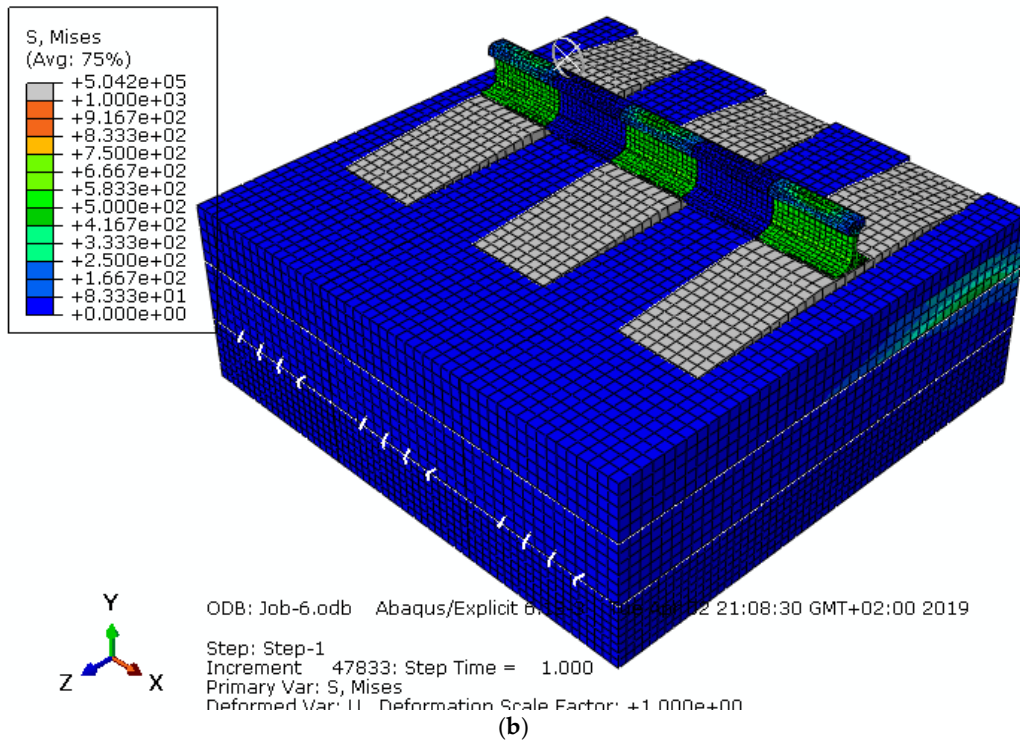
(**b**)

Figure 12. Contours of reduced stress σ^{HM} at the end of the calculation process without reinforcement (**a**) and with geogrid reinforcement (**b**).

(a)

(b)

Figure 13. Contours of strain maps for the end of the surface loading process without reinforcement (**a**) and with geogrid reinforcement (**b**).

4. Experimental Studies Steel of Components

Residual stress values can be obtained by experiments and theoretical analysis. The theoretical analysis of residual stresses is bound up with the elastic theory and elastic properties, plastic flow and material hardening, heat transfer, phase transitions, thermal expansion, structure, and thickness of the surface layer. The experimental stress measurement methods in steel components can be divided into two categories: destructive and non-destructive. Destructive methods do not allow the determination of the quality of tested objects without damage, whereas non-destructive methods allow multiple tests

on the same object. The ultrasonic method used by the authors to determine the residual stresses is based on the relation between ultrasonic wave velocity and stress. Ultrasonic wave velocity is determined with an accuracy of a fraction of a meter per second to measure the residual stresses with the required precision. To measure the absolute values, the effects of temperature and non-uniform distribution of elastic properties and material texture on the wave velocity must be allowed for. A relatively easy and simple method is the ultrasonic measurement with the DEBRO-35 instrument. The method uses electro-acoustic effects, i.e., a relation between stress and velocity or the time the ultrasonic wave requires to cover a specific distance (at the surface). The residual stresses are measured using a special measuring head system that records longitudinal and lateral surface waves (Figure 14).


Figure 14. Measurement of residual stress with a DEBRO instrument.

Experimental rail section tests were performed on components subject to rolling, surface hardening, and three-point and four-point transverse bending of the switch blade I60 used in the railway turnouts. The specimens were bent in the steelworks manufacturing railway turnouts (former Koltram S.A., Zawadzkie, Poland, now TrackTec). For the test new switch blade I60 was used. The length tested of objects were 1275 and 1595 mm.

The three-point and four-point bending process is associated with the production process of railway turnouts (wing rail and switch blade).

The method of section bending including the point of support and force causing strain as well as cross sections was used (see Figure 15). After the selection of measurement places, the residual stress measurement was performed only on the surface of the rail flange and on the top surface of the rail head.

(**a**)   (**b**)
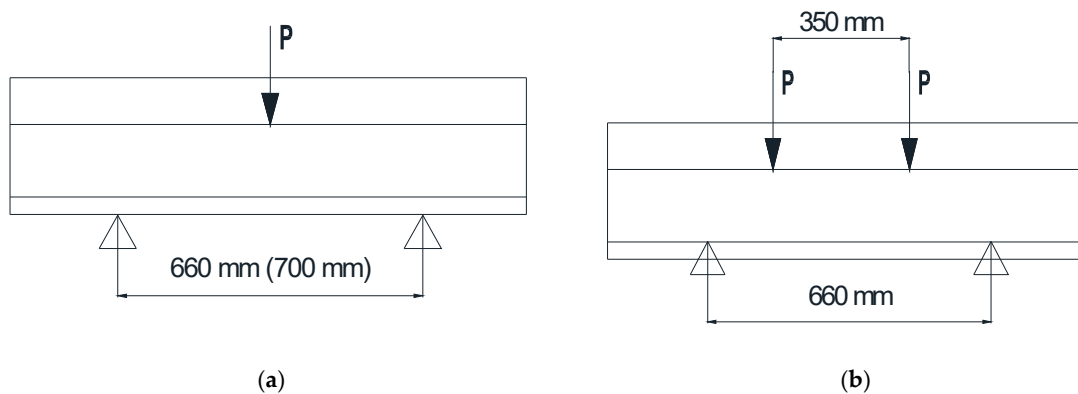
Figure 15. Transverse bending of the switch blade I60—three-point (**a**) and four-point (**b**).

Residual stresses were measured in distances of 0, 150 mm, 300 mm, and 450 mm from both sides of the shores action (point of force application). The stresses on the working surface of a head were measured 5, 10, and 20 mm to the left and right of the center. In turn, the stresses on a food (rail flange) were measured starting from 10 mm from the center, then at 10 mm intervals see (Figures 16–18).
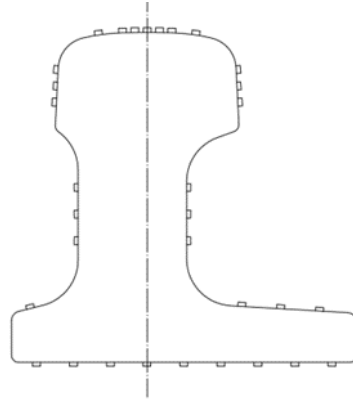

Figure 16. Measurements places at the circumference of rail I60.
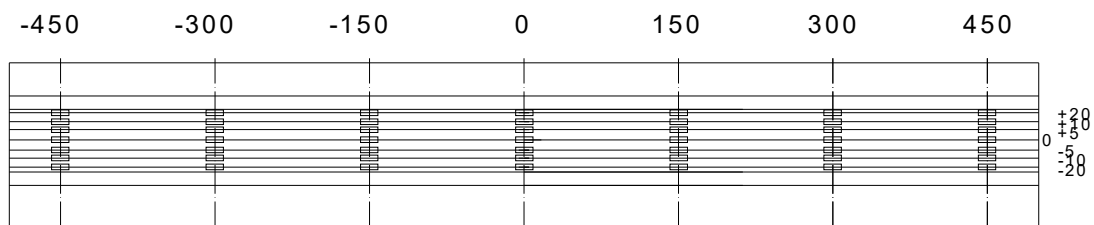

Figure 17. Measurement and cross-section placement on the top surface of the rail head I60.
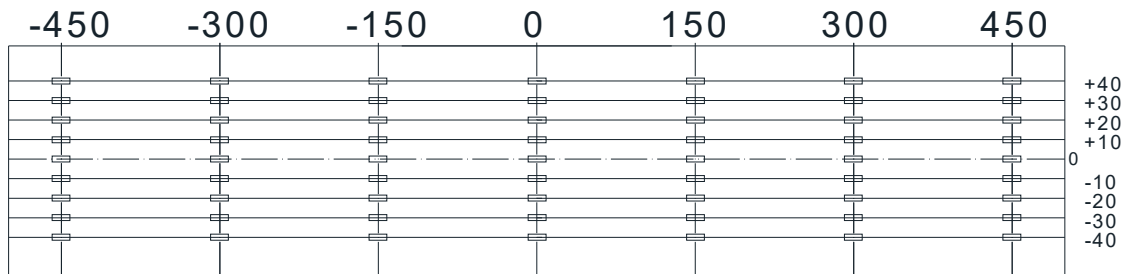

Figure 18. Measurement and cross-section placement on the surface of the rail flange I60.

Figures 19–27 show examples of longitudinal stress on selected parts of rail I60 before and after (three-point and four-point) bending processes and after hardening of selected sections. The horizontal axis represents the longitudinal component of a residual stress and the vertical axis represents the distance from the center of a head rolling surface (measured at the rail a point surface).

Place on the top surface - (0 mm)
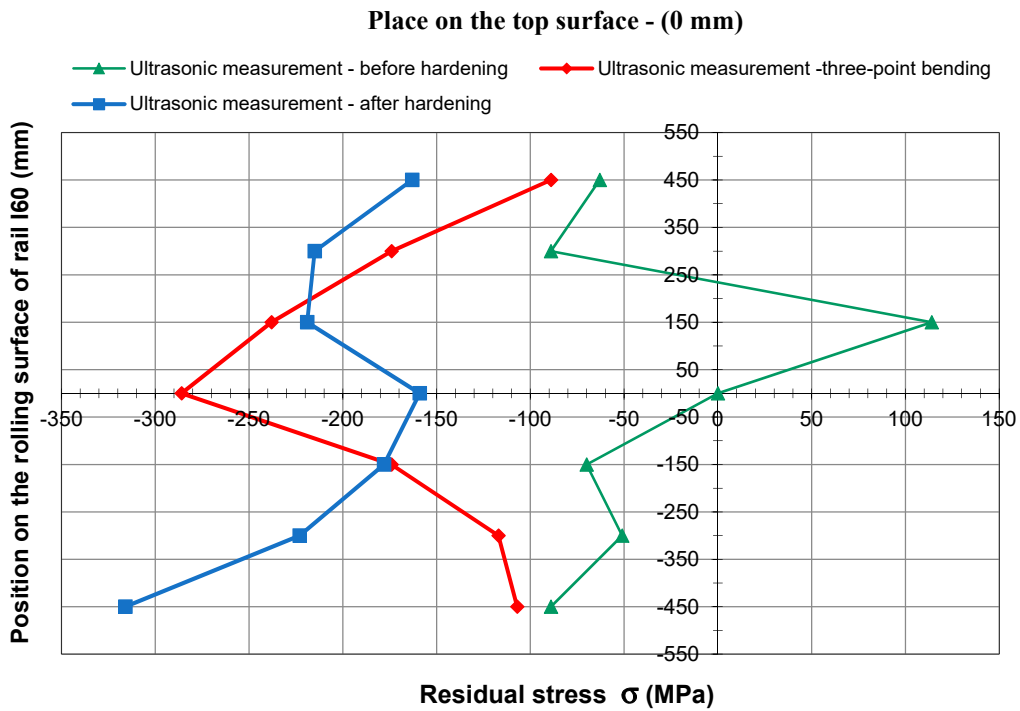
Figure 19. The comparison of results of residual stress changes on the top surface of rail I60 before and after hardening and three-point bending process (section 0 mm).

Place on the top surface - (-5 mm)
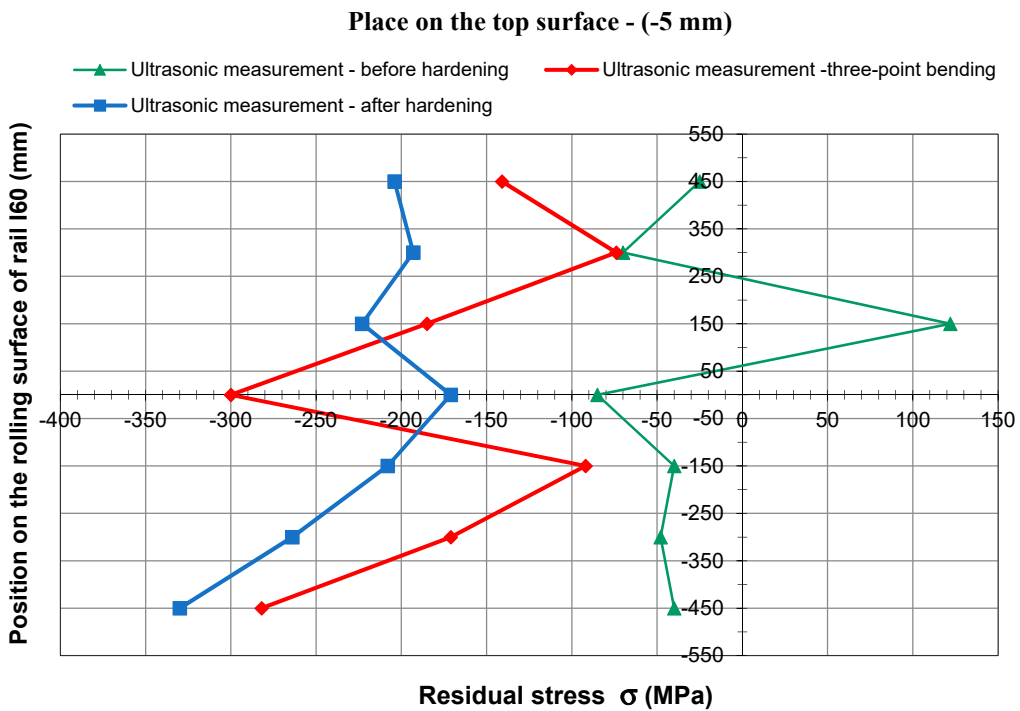
Figure 20. The comparison of results of residual stress changes on the top surface of rail I60 before and after hardening and three-point bending process (section—5 mm).

Place on the top surface - (5 mm)

Figure 21. The comparison of results of residual stress changes on the top surface of rail I60 before and after hardening and three-point bending process (section 5 mm).
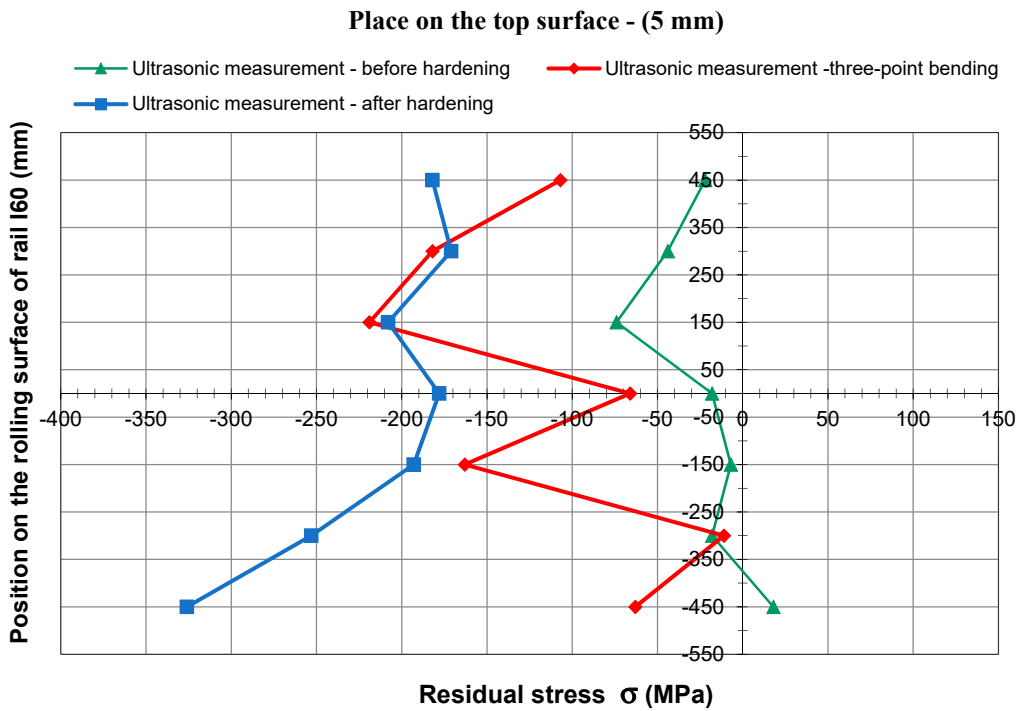
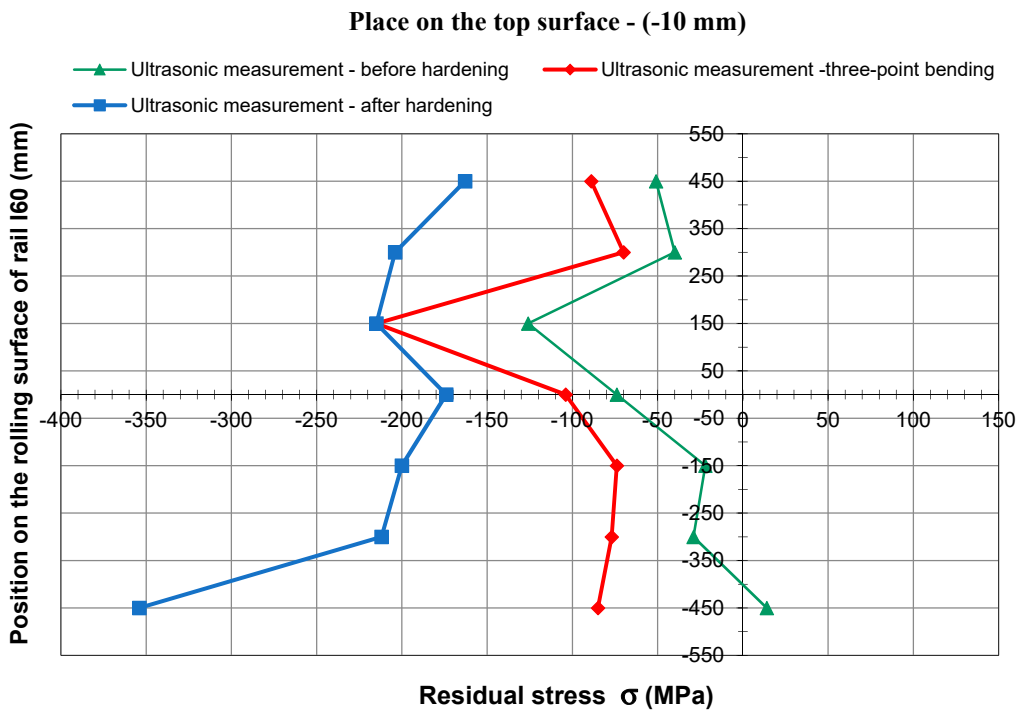**Place on the top surface - (-10 mm)**

Figure 22. The comparison of results of residual stress changes on the top surface of rail I60 before and after hardening and three-point bending process (section—10 mm).

Place on the top surface - (10 mm)

Figure 23. The comparison of results of residual stress changes on the top surface of rail I60 before and after hardening and three-point bending process (section 10 mm).
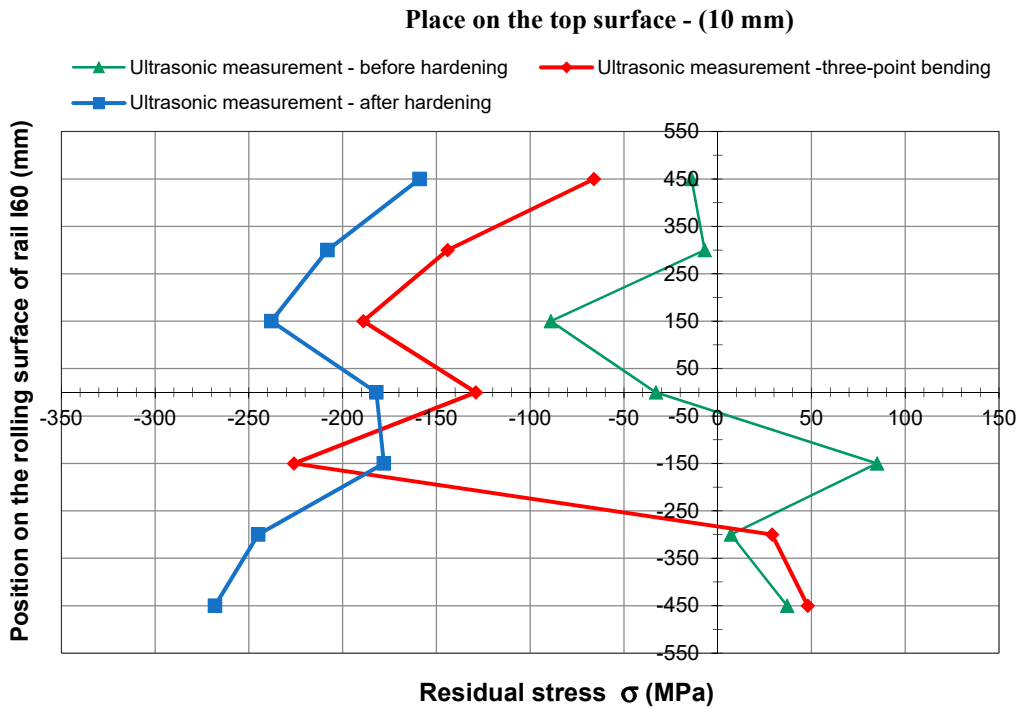
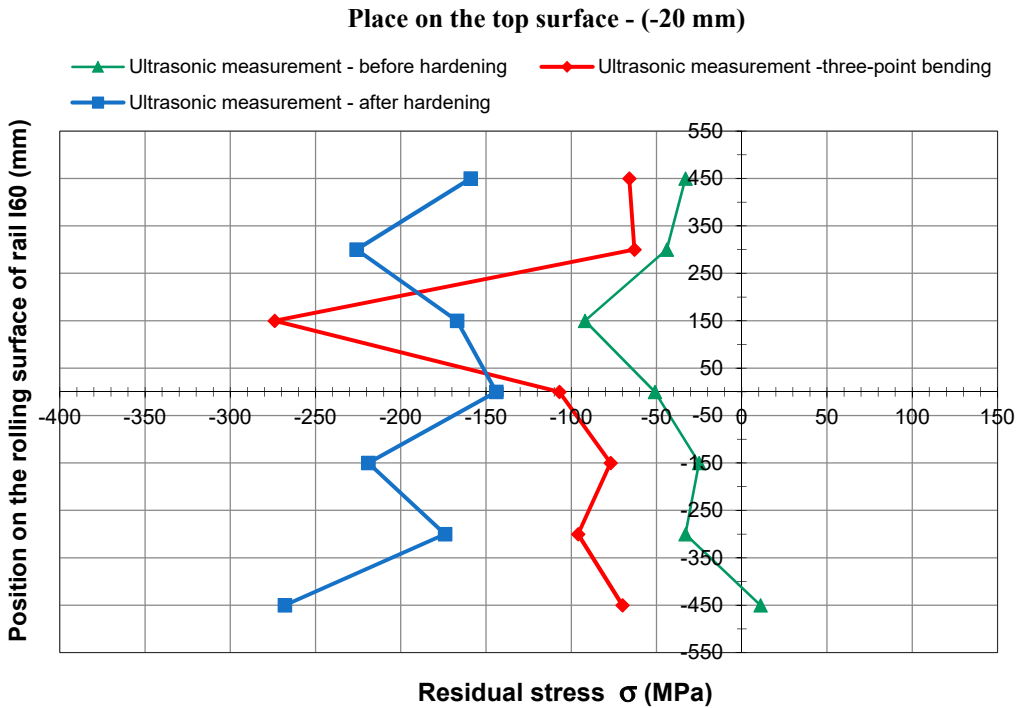**Place on the top surface - (-20 mm)**

Figure 24. The comparison of results of residual stress changes on the top surface of rail I60 before and after hardening and three-point bending process (section—20 mm).

Place on the top surface - (20 mm)

Figure 25. The comparison of results of residual stress changes on the top surface of rail I60 before and after hardening and three-point bending process (section 20 mm).
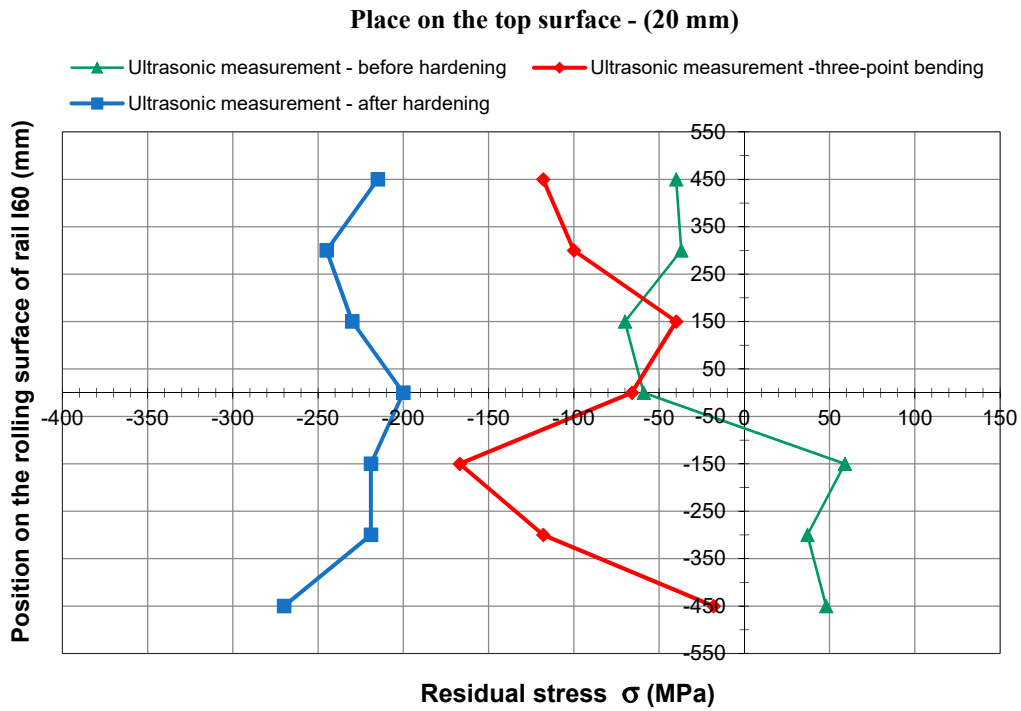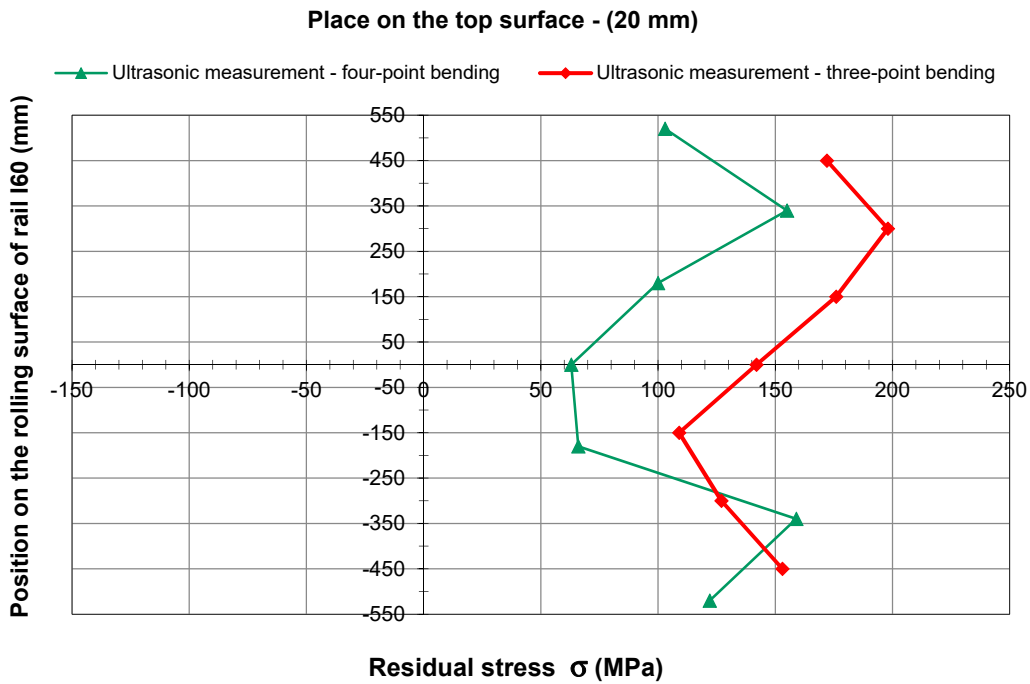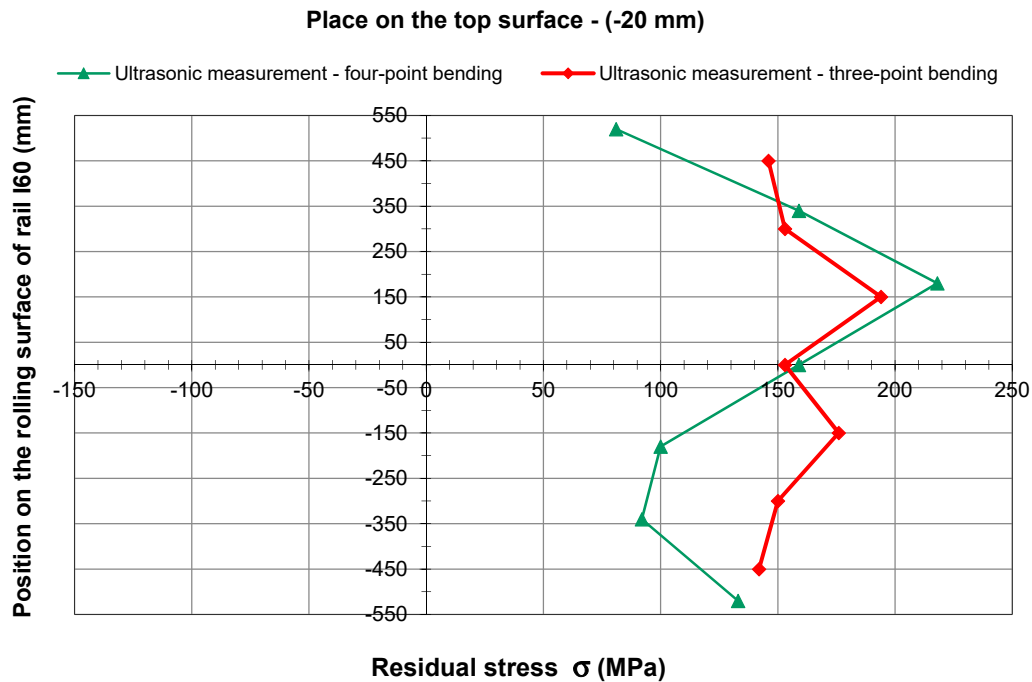
Place on the top surface - (20 mm)

Figure 26. The comparison of results of residual stress changes on the top surface of rail I60 after transverse bending of the rail I60 (three- and four-point)—(section 20 mm).

Place on the top surface - (-20 mm)

Figure 27. The comparison of results of residual stress changes on the top surface of rail I60 after transverse bending of the rail I60 (three- and four-point)—(section—20 mm).

Figures 26 and 27 show the comparison of results of the measurement of residual stress by an ultrasonic instrument after transverse bending of the rail I60 (three- and four-point).

For better readability and transparency of selected experimental and numerical results, a summary of them was presented in one figure. The comparison includes the results obtained for three- and four-point bending processes. This is a preliminary validation of the obtained results of the numerical tests.

Figures 28 and 29 present a comparison of selected simulation results with the results of the ultrasonic measurements for comparable conditions and measuring places.

Presented results of measurements of residual stresses by ultrasonic method show how technological process can affect the size and distribution of residual stresses. The differences are visible on the example of three-point and four-point bending (Figures 26–29). Differences in residual stresses in the same cross-sections and measuring places after a four-point bending are in some cases lower by 100 MPa in relation to three-point bending. In turn, the results of measurements after surface hardening presented in Figures 19–25 show that toughening introduces into the system an element of compressive stress reaching 350 MPa. Compressive stresses from the point of view of exploitation are very advantageous because they prevent the formation of microcracks on the surface of the element. The comparison of measurement results with the results of numerical calculations indicates their qualitative compatibility (Figures 28 and 29). Quantitative discrepancy between measurements and simulation calculations may result from too idealized and simplified boundary conditions in the numerical model. It should be noted that the numerical calculations do not take into account the residual stresses usually occurring in rails in the initial state (before bending). These stresses occur as a result of technological processes, especially the straightening of the rail in the roller straightening machine

Place on the top surface - (0 mm)
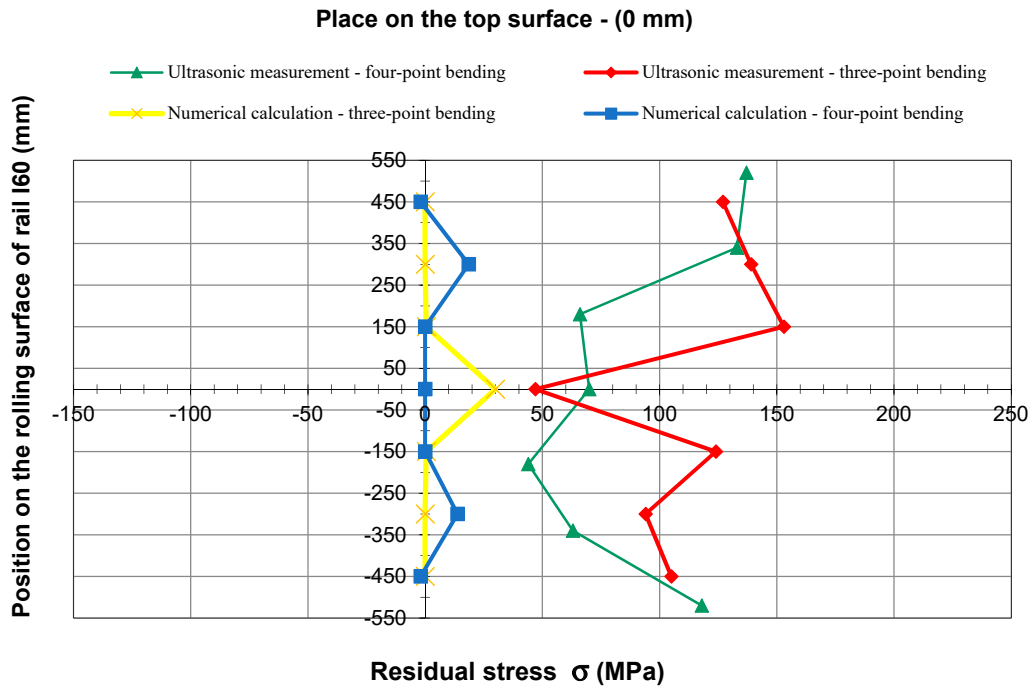
Figure 28. The comparison of results of the measurement of residual stress and numerical calculation after three- and four-point bending (section—0 mm).

Place on the top surface - (10 mm)
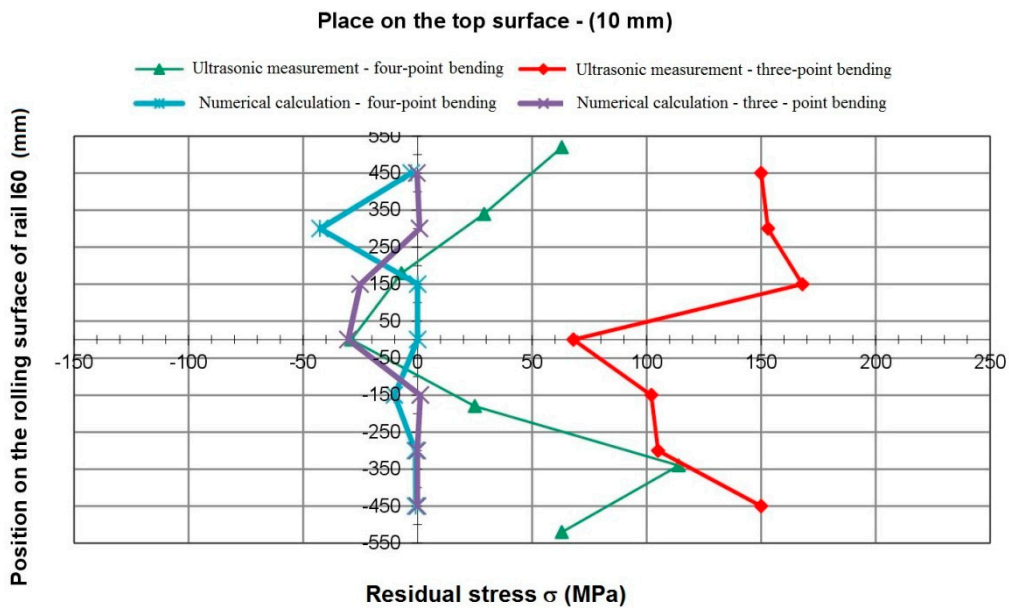
Figure 29. The comparison of results measurement of residual stress and numerical calculation after three- and four-point bending (section—20 mm).

5. Experimental Studies of Superstructure

The objects of the experimental test solution were developed by the Department of Transport Infrastructure of Warsaw University of Technology Faculty of Transport [25]. Proposed crushed stone composite comprises a layer of crushed stone reinforced with two geogrids and stabilized with a polyurethane resin (Figure 30). It is characterized by the mechanical and chemical resistance of the ballast to the phenomenon of deconsolidation.
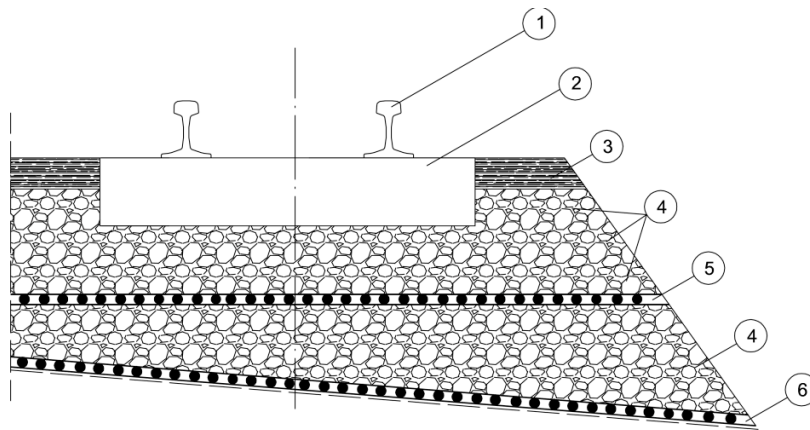
**Figure 30.** Track structures with crushed stone composite [45] (**1**) rail UIC 60 (60E1), (**2**) sleeper, (**3**) crushed stone layer with resin, (**4**) ballast, (**5**) top reinforcement (geogrid, geosynthetic), (**6**) bottom reinforcement (geogrid, geosynthetic).

A track substructure with a crushed stone composite is a solution of reinforced standard track substructure to reduce deconsolidation ballast. Deconsolidation means the concentration of ballast, increasing its volume. Mechanical proofing consists of reinforcing the ballast bed with two geogrids. Limiting the increase in volume of the ballast pile is a precondition for limiting the phenomenon of deconsolidation. The bottom reinforcement consists of geogrid or geosynthetic [5,6] laid at the top of the subgrade (Figure 30). Resin, after its concentration, penetrates into the meshes of the geogrids providing mechanical anchoring of the aggregate. The meshes make the structure of the bald stone more homogeneous and increase the angle of internal friction of the ballast. Finally, crushed stone areas exposed to strong vibrations are stabilized chemically. The penetration by the binder should not go deeper than one half of the height of the sleeper (80 mm), to enable breaking up crushed stone composite with a tamping machine.

The experimental track section with crushed stone composite was built on the Central Trunk Line in 2008. Given the local environment, the experimental section was built using an AHM Formation rehabilitation machine for plain track with two excavating chains and integrated material recycling) machine, which enables laying and compacting the subgrade layer within a single pass, while the other pass builds and compacts the new ballast bed and lays crushed stone reinforcing the geogrids. The experimental section was divided into four sectors and plots shown in Figure 31.
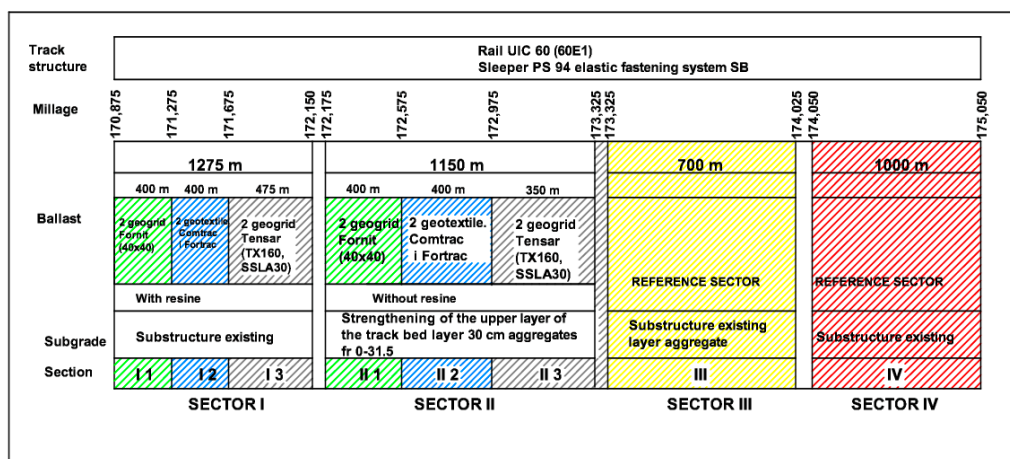
Figure 31. Diagram of the experimental section of track with crushed stone composite on the Central Trunk Line [24].

Unfortunately, experimental studies did not include simulation studies involving strains and stresses. The analyzed test section was subjected to test, on which the geometrical deformability of the track was tested during operation. The main goal of the measurement of geometric position of the track on the sections with the crushed stone composite was to assess its deformability during operation compared to the classic track (reference sector) on the adjacent section of the track. Results of the EM 120 (measuring motor car) measurements during 18 trips made between 2008 and 2014 were used in the evaluation of track geometry deformability. The traffic load in that period was approx. 20 Tg. Selected results of averaged measurement values of standard deviation for vertical irregularities is shown in Figures 32–34. The difference is that the reference sector has been prepared without additional surface reinforcements (types of geogrids and a crushed stone layer with resin). Such a solution is a standard solution performed in modernization works or the construction of new sections of the railway line.
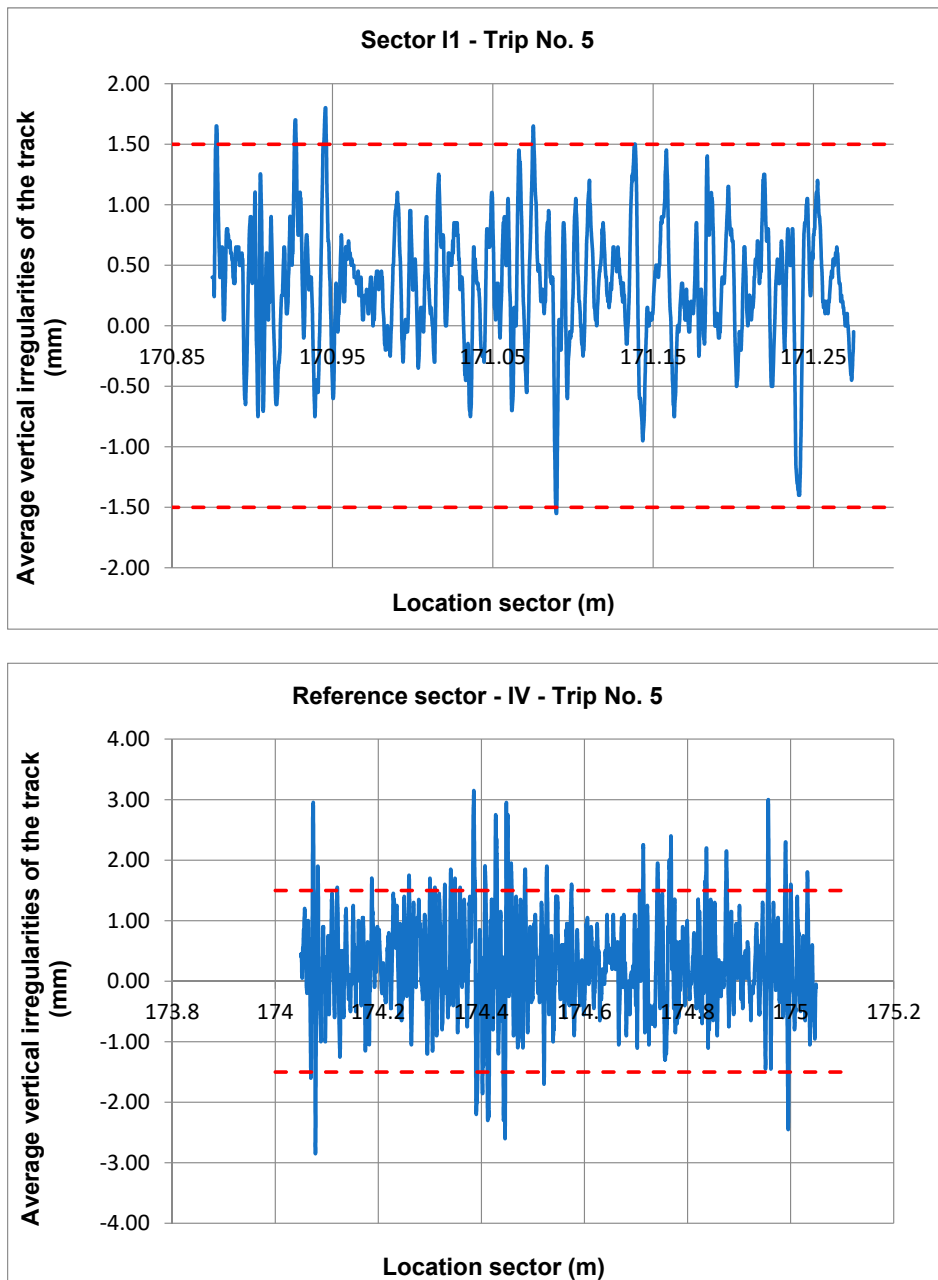

Figure 32. The average vertical irregularities of the reference sector IV and sector I1—trip No. 5.
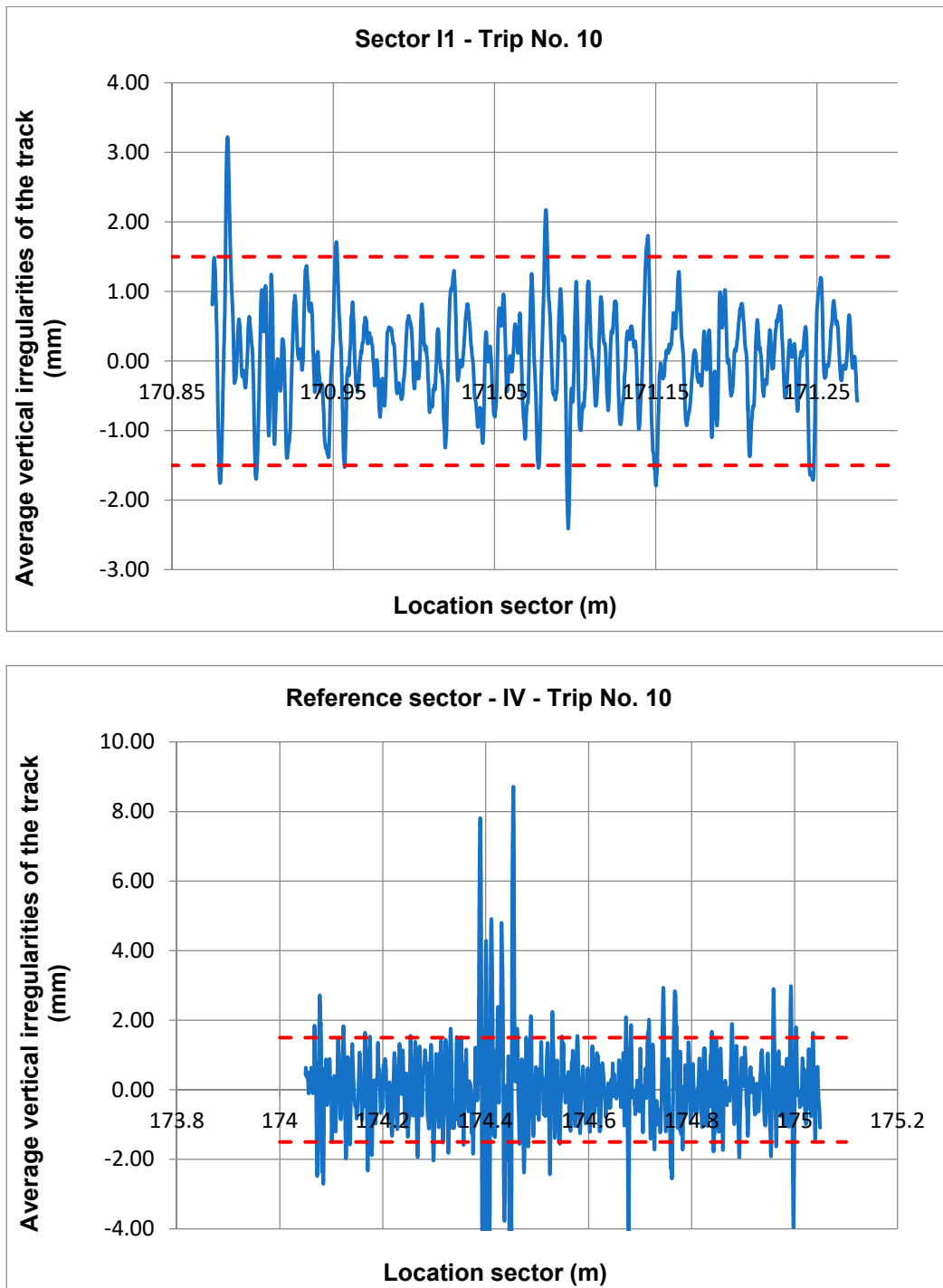
Figure 33. The average vertical irregularities of the reference sector IV and sector I1—trip No. 10.
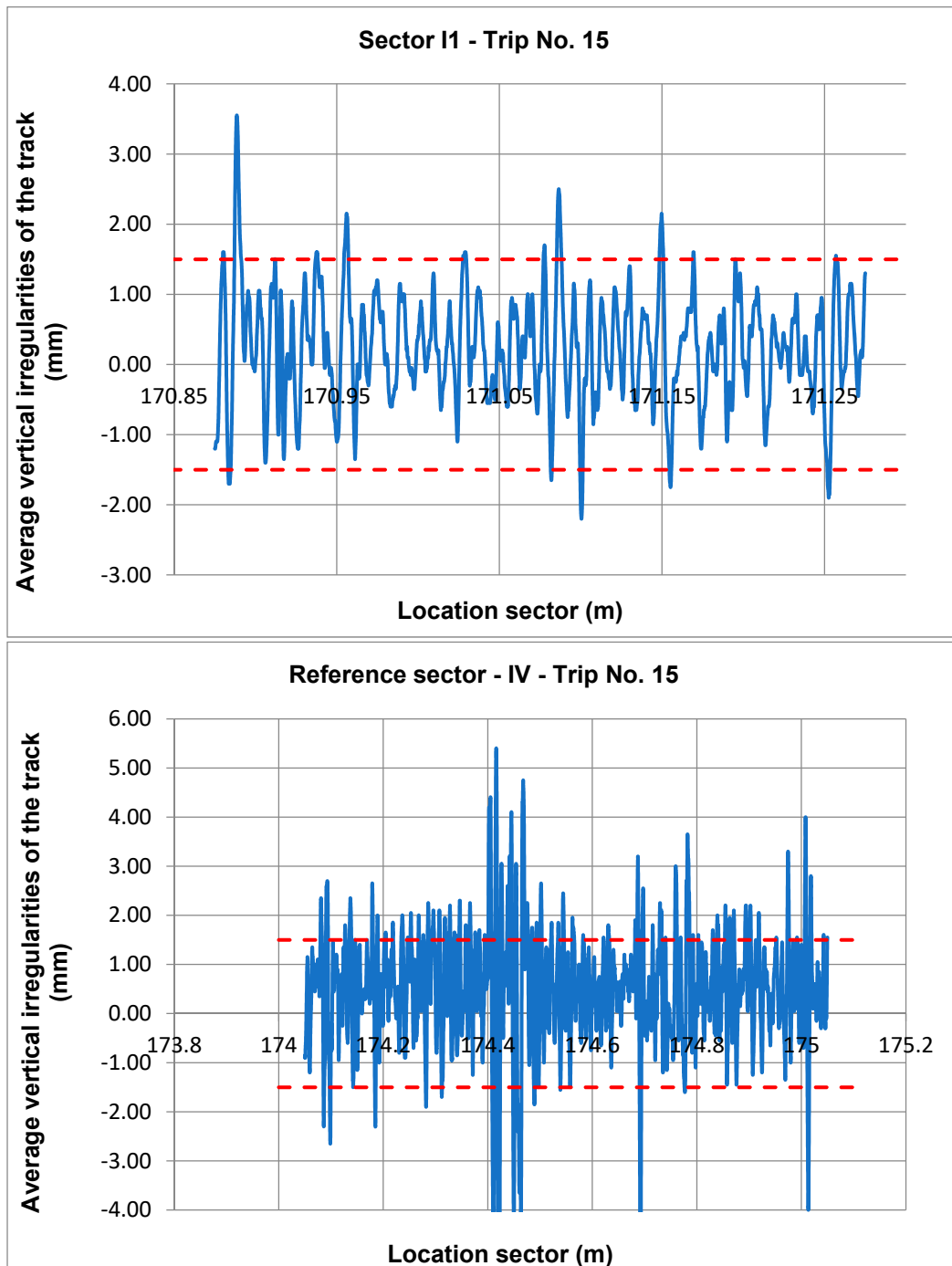
Figure 34. The average vertical irregularities of the reference sector IV and sector I1—trip No. 15.

6. Summary

This paper presents two research problems:

- rail traffic safety associated with residual stress in steel elements
- reducing railway track operating costs

For the first problem, it is believed that the fatigue crack growth in railway rails is greatly influenced by the residual stress states. The main sources of residual stresses in rails are: the manufacturing process (cooled rolling and straightening), rolling wheels of railroad cars, and transverse bending used in cold forming of switch blades. In the second problem, the optimization of the maintenance costs by

using advanced solutions in the track superstructure design may be an interesting method to extend its durability and to extend the time between repairs.

Both problems are related to simulation and experimental research. The finite element method was used in simulation tests and is presented in this paper. It confirms that the FEM is a tool that can be used to determine the propriety of a proposed solution or to simulate a technological or production process of the railway turnout elements. It is a solution that is less expensive than conducting experimental research, but it should not be treated as the only one in the research. It should be emphasized that prepared simulation models should be verified by other simulation tools or additional experimental tests. This will enable verification of assumptions and improvement of simulation models.

The presented models are still not perfect and require work. An example is the comparison of the results of the simulation and experimental tests of the production processes (bending and hardening). Numerical calculations do not take into account residual stresses usually occurring in rails in the initial state (before bending).

The results of the simulation tests presented in this paper were compared with results of experimental tests. This applies mainly to the test of residual stresses in elements of steel railway turnouts and a new solution to reinforce the structure of the railway surface. Their scope was limited due to the costs and long time required for experimental research. Unfortunately, experimental studies did not include a range of tests such as simulation studies involving strains and stresses. The analyzed test section was subjected to testing, on which the geometry deformability of the track was tested during operation. Presented numerical research will be continued and will be extended with new simulation tools using discrete elements (DEM), suited for the simulation of elements such as aggregate ballast. These tools will be able to supplement the research and will also validate results obtained for the FEM. Presented research results are an inspiration to continue research in this area and to search for new solutions, including optimizing the costs of maintaining the railway transport infrastructure and determining the viability of the structure using simulation methods.

Conflicts of Interest: The authors declare no conflicts of interest.

References

1. Mikulski, J.; Gorzelak, K. Conception of modernization of a line section example in the context of a fast railway connect. *Arch. Transp.* **2017**, *44*, 47–54. [CrossRef]
2. Szeląg, A. Electrical power infrastructure for modern rolling stock with regard to the railway in Poland. *Arch. Transp.* **2017**, *42*, 75–83. [CrossRef]
3. Burdzik, R.; Nowak, B.; Rozmus, J.; Słowiński, P.; Pankiewicz, J. Safety in the railway industry. *Arch. Trans.* **2017**, *44*, 15–24. [CrossRef]
4. Jacyna, M.; Gołębiowski, P.; Urbaniak, M. Multi-option Model of Railway Traffic Organization Including the Energy Recuperation. *Model. Simul.* **2016**, *640*, 199–210.
5. Peixoto, D.F.C.; Ferreira, L.A.A. Linear analysis of the wheel/rail contact. In Proceedings of the CTF2010—First International Congress on Rail Transport Technology, Zaragoza, Spain, 12–14 April 2010.
6. Plasek, O.; Hruzikova, M. Design of under sleeper pads for Turnout. *Arch. Inst. Inż. Lądowej Politech. Pozn.* **2007**, *3*, 241–249.
7. Zienkiewicz, O.C.; Taylor, R.L.; Nithiarasu, P.; Zhu, J.Z. *The Finite Element Method*; McGraw-Hill: New York, NY, USA, 1977.
8. Liu, W.N.; Zhang, Y.Q. A periodic analytical solution of railway track structure under moving loads. *Eng. Mech.* **2004**, *5*, 100–102.

9.   Ergenzinger, C.; Seifried, R.; Eberhard, P. A discrete element approach to model breakable railway ballast. *J. Comput. Struct.* **2012**, *7*, 41010. [CrossRef]

10. Ižvolt, L.; Dobeš, P.; Pieš, J. Verification of boundary conditions of numerical modeling of the track substructure thermal regime influence of the snow cover. *Arch. Transp.* **2018**, *4*, 51–60. [CrossRef]

11. Leykauf, G.; Lechner, B.; Stahl, W. *Improved Ballasted Track for Speed Lines*; Rail Engineering: London, UK, 2004.

12. Desai, C.S.; Siriwardane, A.M. Numerical models for track support structures. *J. Geotech. Eng. Div.* **1982**, *108*, 461–480.

13. Mohammadi, M.; Karabalis, D.L. Dynamic 3D soil railway track interaction by BEM–FEM. *Earthq. Eng. Struct. Dyn.* **1995**, *24*, 1177–1193. [CrossRef]

14. Song, M.K.; Noh, H.C.; Choi, C.K. A new three-dimensional finite element analysis model of high-speed train–bridge interactions. *Eng. Struct.* **2003**, *25*, 1611–1626. [CrossRef]

15. Biempica, C.B.; Del Coz Diaz, J.J.; Nieto, P.G.; Sanchez, I.P. Nonlinear analysis of residual stresses in a rail manufacturing process by FEM. *Appl. Math. Model.* **2009**, *33*, 34–53. [CrossRef]

16. Guerice, W.; Heller, W.; Kasprowicz, J.; Weisse, M. Verbesserte Bruchsicherheit von Schienen durch optymiertes Rollenrichten. *Eisenb. Rundsch.* **2001**, *50*, 541–551.

17. Guerice, W.; Weiser, J.; Schmedders, H.; Dannenberg, R. Ursachen von Schienen-Eigenspannungen Infolge Rallrichtens und Beitrag zur Verriungerung. *Eisenbahntechnische Rundschau* **1997**, *46*, 655–662.

18. Bogdański, S.; Olzak, M.; Stupnicki, J. Numerical stress analysis of rail rolling contact fatigue cracks. *Opt. Lasers Eng.* **1997**, *27*, 89–100. [CrossRef]

19. Kukulski, J. Distribution of residual stresses of railway superstructure steel components after the rolling processes. *Prz. Komun.* **2011**, *9*, 74–78. (In Polish)

20. Gisterek, I.; Krużyński, M. Chemical stabilization of the ballast on the railway lines. *Prz. Komun.* **2009**, *9*, 36–39. (In Polish)

21. Nowakowski, T.; Komorski, P.; Tomaszewski, F. The efficiency of tram articulations compared to vibroacoustic emissions. *Arch. Transp.* **2017**, *44*, 55–63. [CrossRef]

22. Lundgren, J.R.; Martin, G.C.; Hay, W.W. *A Simulation Model of Ballast Support and the Modulus of Track Elasticity*; Civil Engineering Studies, Transportation Series, No. 4; University of Illinois at Urbana-Champaign: Champaign, IL, USA, 1970.

23. Shan, Y.; Albers, B.; Savidis, S.A. Influence of different transition zones on the dynamic response of track–subgrade systems. *Comput. Geotech.* **2013**, *48*, 21–28. [CrossRef]

24. UIC. ORE D 182 Unified Assessment Criteria for Ballast Quality and Methods for Assessing the Ballast Condition in the Track. In *Determining the Criteria for Ballast Durability Using Triaxial Tests, Utrecht*; UIC: Chicago, IL, USA, 1994.

25. Basiewicz, T.; Gołaszewski, A.; Kukulski, J.; Towpik, K. Tests on a Track Structure with Crashed Stone Composite on an Experimental Section of the CMK (Central Trunk Line). *J. Civ. Eng. Archit. Res.* **2016**, *3*, 1220–1227.

26. Lei, X.; Chen, S. Space dynamic analysis of track structure of high speed railway. *Traffic Transp. Stud.* **2000**, *2000*, 770–775.

27. Lei, X.; Zhang, B. Analysis of dynamic behavior for slab track of high-speed railway based on vehicle and track elements. *J. Transp. Eng.* **2010**, *137*, 227–240. [CrossRef]

28. Zhang, Q.; Zhu, X.; Wang, L. Track Allocation Optimization in Multi-Direction High-Speed Railway Stations. *Symmetry* **2019**, *11*, 459. [CrossRef]

29. Zobel, H.; Al-Khafaji, T.; Wróbel, M.; Żółtowski, P.; Papis, B.; Sulik, P.; Dec, L. Zastosowanie podkładów z kompozytów polimerowych w budownictwie infrastrukturalnym. Zeszyty Naukowo-Techniczne Stowarzyszenia Inżynierów i Techników Komunikacji w Krakowie. *Ser. Materiały Konf.* **2017**, *112*, 197–221.

30. Szcześniak, W.; Hypki, M.; Skulski, B.; Śledziewski, K. Static and dynamic load test of a shell-soil bridge. *Logistyka* **2014**, *6*, 10252–10261. (In Polish)

31. Tanabe, M.; Wakui, H.; Matsumoto, N.; Okuda, H.; Sogabe, M.; Tanabe, Y. *Dynamic Interactions of Shinkansen Train, Track and Bridge*; IABSE: Zürich, Switzerland, 2003.

32. Tajduś, A.; Cała, M.; Tajduś, K. *Geomechanika w Budownictwie Podziemnym: Projektowanie i Budowa Tuneli*; Wydawnictwa AGH: Kraków, Poland, 2012. (In Polish)

33. Bętkowski, P. Przebudowa i zabezpieczenie przed wpływami górniczymi niewielkiego wiaduktu kolejowego zintegrowanego z nasypem. *Prz. Gór.* **2015**, *71*, 1–7.

34. Shahu, J.; Yudhbir; Kameswararao, N. A Rational Method for Design of Railroad Track Foundation. *Soils Found.* **2000**, *40*, 1–10. [CrossRef]

35. Markin, V.L.; De Man, A.P.; Esveld, C. A procedure for design and optimization of a railway track structure. In Proceedings of the UIC Interactive Conference, Paris, France, 8–9 December 1998.

36. Dietz, S.; Hippmann, G.; Schupp, G. Interaction of vehicles and flexible tracks by co-simulation of multibody vehicle systems and finite element track models. *Veh. Syst. Dyn.* **2002**, *37*, 372–384. [CrossRef]

37. ORE. *Question D71; Stresses in the Rails, the Ballast and in the Formations Resulting from Traffic Load, Report no.12*; Repeated loading of Clay and Track Foundation Design, Report no. D71/RP12; Office for Research and Experiments-International Union of Railways Utrecht: Utrecht, The Netherlands, 1970.

38. Esveld, C. Law maintenance ballastless track structures. *Rail Eng. Int. Ed.* **1997**, *26*, 3.

39. Sakdirat, K.; Alex, M. Remennikov Impact Capacity of Railway Prestressed Concrete Sleepers. *IES J. Part A Civ. Struct. Eng.* **2009**, *2*, 47–58.

40. Eisenmann, J.; Kaess, G. Das Verhalten des Schotters unter Belastung. *Eisenbahntechnische Rundschau* **1980**, *3*, 201–208.

41. Eisenmann, J. Qualitat des Oberbauzustandes. *Der Eisenbahningenieur* **1980**, *31*, 73–89.

42. Eisenmann, J. Verhaltensfunktion des Schotters, Folgerungen fur hohe Fahrgeschwindigkeiten. *Der Eisenbahningenieur* **1981**, *12*, 100–103.

43. Giannakos, K.; Loizos, A. Ballast stressing on a railway track and the behaviour of limestone ballast. In *Advances in Transportation Geotechnics*; Taylor & Francis Group: London, UK, 2008; pp. 577–585.

44. González-Nicieza, C.; Álvarez-Fernández, M.I.; Menéndez-Díaz, A.; Álvarez-Vigil, A.E.; Ariznavarreta-Fernández, F. Failure analysis of concrete sleepers in heavy haul railway tracks. *Eng. Fail. Anal.* **2008**, *15*, 90–117. [CrossRef]

45. Kukulski, J. Experimental and simulation study of the superstructure and its components. In *Railway Research—Selected Topics on Development Safety and Technology*; Zboinski, K., Ed.; IntechOpen Limited: London, UK, 2015; pp. 115–143.

46. Dong, Y.L.; Han, J.; Bai, X.H. Numerical analysis of tensile behavior of geogrids with rectangular and triangular apertures. *Geotext. Geomembr.* **2011**, *29*, 83–91. [CrossRef]

47. Huang, H.; Tutumluer, E. Discrete Element Modelling for fouled railroad ballast. *Constr. Build. Mater.* **2011**, *25*, 3306–3312. [CrossRef]

48. Lim, W.L.; McDowell, G.R. Discrete element modelling of railway ballast. *Granul. Matter* **2005**, *7*, 19–29. [CrossRef]

49. Lobo-Guerrero, S.; Vallejo, L.E. Discrete element method analysis of railtrack ballast degradation during cyclic loading. *Granul. Matter* **2006**, *8*, 195–204. [CrossRef]

50. *ABAQUS–Standard User's Manual, Hibbitt*; Karlsson and Sorensen, Inc.: New York, NY, USA, 2000.